Multiscale impact of nucleotides and cations on the conformational equilibrium, elasticity and rheology of actin filaments and crosslinked networks

Multiscale impact of nucleotides and cations on the conformational equilibrium, elasticity and rheology of actin filaments and crosslinked networks

Tamara Carla Bidone[1,*], Taeyoon Kim[2], Marco A. Deriu[3], Umberto Morbiducci[1], Roger D. Kamm[4]

[1]Department of Mechanical and Aerospace Engineering, Politecnico di Torino, corso Duca degli Abruzzi 24, 10129, Torino, Italy
[2]Weldon School of Biomedical Engineering, Purdue University, 206 S. Martin Jischke Drive, West Lafayette, IN 47907-2032, USA
[3]Department of Innovative Technologies, University of Applied Science of Southern Switzerland, Galleria 2, 6928 Manno, Switzerland
[4]Departments of Biological and Mechanical Engineering, Massachusetts Institute of Technology, 77 Massachusetts Avenue, Cambridge, MA 02139-4307, USA

[*]currently: Department of Physics, Lehigh University, Bethlehem, PA 18015, USA

[4]To whom correspondences should be addressed. Email: rdkamm@mit.edu. Telephone: (617) 253-5330. Fax: (617) 258-8559.

ABSTRACT

Cells are able to respond to mechanical forces and deformations. The actin cytoskeleton, a highly dynamic scaffolding structure, plays an important role in cell mechano-sensing. Thus, understanding rheological behaviors of the actin cytoskeleton is critical for delineating mechanical behaviors of cells. The actin cytoskeleton consists of interconnected actin filaments (F-actin) that form via self-assembly of actin monomers. It has been shown that molecular changes of the monomer subunits impact the rigidity of F-actin. However, it remains inconclusive whether or not the molecular changes can propagate to the network level and thus alter the rheological properties of actin networks. Here, we focus on how cation binding and nucleotide state tune the molecular conformation and rigidity of F-actin and a representative rheological behavior of actin networks, strain-stiffening. We employ a multiscale approach by combining established computational techniques: molecular dynamics, normal mode analysis, and Brownian dynamics. Our findings indicate that different combinations of nucleotide (ATP, ADP or ADP-Pi) and cation (Mg^{2+} or Ca^{2+} at one or multiple sites) binding change the molecular conformation of F-actin by varying inter- and intra-strand interactions which bridge adjacent subunits between and within F-actin helical strands. This is reflected in the rigidity of actin filaments against bending and stretching. We found that differences in extension and bending rigidity of F-actin induced by cation binding to the low-, intermediate- and high-affinity sites vary the strain-stiffening response of actin networks crosslinked by rigid crosslinkers, such as scruin, whereas they minimally impact the strain-stiffening response when compliant crosslinkers, such as filamin A or α-actinin, are used.

Keywords
actin, filament, network, rheology, cation, multiscale model

INTRODUCTION

The cytoskeleton is an interconnected network of filamentous semiflexible polymers regulating the responses of cells to external deformations (Wang et al. 1993; Bausch et al. 1999). Actin is the most abundant protein of the cytoskeleton and is deeply involved with cell mechano-sensing. Actin undergoes transitions between monomeric (G-actin) and filamentous states (F-actin) during processes such as changes in cell shape and migration (Korn et al. 1987; Borisy and Svitkina 2000; Bunnell et al. 2001). During these transitions, the microstructure of F-actin, a double-stranded helix consisting of monomer subunits, experiences conformational rearrangements owing to polymerization, nucleotide hydrolysis and cation exchanges at multiple sites (Cooper et al. 1983; Estes et al. 1987; Zimmerle et al. 1987; Méjean et al. 1988; Strzelecka-Gołaszewska et al. 1993; Strzelecka-Golaszewska et al. 1996; Moraczewska et al. 1996; Moraczewska et al. 1999; Guan et al. 2003). The inherent coupling between actin subunit conformation and the rigidity of actin filaments and networks makes it critical to explore actin conformations responsible for different mechanical behaviors of cells.

Each monomer subunit along F-actin has a nucleotide binding site, a high-affinity cation-binding site (Estes et al. 1992a) and at least three intermediate- and low-affinity divalent-cation-binding sites (Zimmerle et al. 1987) (Fig. 1a). In physiological conditions, actin exists in multiple conformations, bound to one or several cations and with either ATP, ADP or intermediate ADP-Pi, and exhibits various filament properties. For example, the dynamics (Korn et al. 1987; Estes et al. 1992a) and rigidity of F-actin (Kang et al. 2012) are altered by ATP hydrolysis and cation exchanges. Also, a significant correlation exists between ATP hydrolysis and the type of cation bound to the high-affinity site (Carlier et al. 1986; Carlier et al. 1987; Estes et al. 1992b). It was shown that upon exchange of Ca^{2+} for Mg^{2+} at the high-affinity binding site, the nucleotide-binding cleft tends to be open (Nyitrai 1999), whereas Ca^{2+} induces a bridge of increased density between the two strands of F-actin (Orlova and Egelman 1995). With binding of multiple cations at the low- and intermediate-affinity sites, the interface area of monomer subunits increases due to lower electrostatic repulsions between adjacent subunits (Janmey 1996; Shi et al. 2007), and the number of inter-monomer contacts also increases (De La Cruz et al. 2010). One area of interest is the hypothesis that different molecular conformations of the subunits favor specific inter-subunit interactions which in turn affect macroscopic filament properties (Chu and Voth 2006a; Pfaendtner et al. 2010; De La Cruz et al. 2010; Saunders and Voth 2012). Previous studies have shown that molecular-level heterogeneities in both the dynamics of a single subunit and the interactions between subunits along the filaments are critical to filament rigidity (Fan et al. 2012). It is likely that cation binding, at low-, intermediate-, and high-affinity sites, and nucleotide hydrolysis complementarily affect the molecular heterogeneity and macroscopic stiffness of F-actin, and that this impacts the rheology of crosslinked actin networks. We previously demonstrated that the stiffness of F-actin is controlled by rearrangements of specific groups of residues in the subunits, as they weaken or stabilize monomer-to-monomer interactions (Deriu et al. 2011), but we did not consider the different configurations of the F-actin with nucleotides and nucleotide/cation(s) binding.

Within cells, F-actins are crosslinked into a network by various crosslinking proteins such as α–actinin (Xu et al. 2000), filamin A (Gardel et al. 2006b; Schmoller et al. 2009) and scruin (Shin et al. 2004), whose density, binding activity, and mechanical properties modulate the network viscoelasticity (Schnurr et al. 1997; Tseng et al. 2002; Gardel et al. 2006a; Tharmann et al. 2007; Schmoller et al. 2009; Lieleg et al. 2009; Kim et al. 2009b; Lieleg et al. 2010; Unterberger et al.

2013). Properties of F-actin including concentration and mechanical stiffness can also play an important role in modulating network elasticity (MacKintosh et al. 1995; Grooman et al. 2012). Indeed, we demonstrated that variations in extensional and bending stiffnesses of F-actin highly affect the shear modulus of a crosslinked network (Kim et al. 2009b). Therefore, binding of cations and nucleotides can impact not only the molecular conformation and stiffness of the F-actin but also have potential to affect mechanical behaviors of crosslinked actin networks.

Despite the previous efforts, how the conformational rearrangements of monomer subunits and F-actins propagate from the molecular level up to the network level is still unclear. Here, we hypothesized that cation binding and nucleotide hydrolysis complementarily affect F-actin stiffness and that this, in turn, impacts a representative rheological behavior of crosslinked actin networks, strain-stiffening. To test the hypothesis, we employed a multiscale approach by combining three computational models, spanning length and time scales from angstroms to micrometers and from nanoseconds to seconds. By applying the multiscale model, we investigated how molecular differences resulting from various combinations of nucleotide and cation(s) may propagate from monomer subunits to F-actin and tune F-actin mechanics and how these affect strain-stiffening of a crosslinked actin network. In detail, we examined (1) whether changes in bending and extensional rigidity of F-actin are correlated with the equilibrium conformation resulting from binding of cations at the low-, intermediate- and/or high-affinity site in different nucleotide forms; (2) whether these changes in F-actin rigidity impact the strain-stiffening of crosslinked actin networks.

METHODS

In this study, for a multiscale computational approach, (1) at the atomistic level, we used equilibrium molecular dynamics (MD) simulations in order to predict the conformational modifications of subunits along F-actin induced by binding of one or more cations in various nucleotide states; (2) at the filament level, we applied the anisotropic network model (ANM) together with the rotation translation block (RTB) approach in order to compute bending and extensional rigidities of F-actin; (3) at the network level, we conducted Brownian dynamics (BD) simulations of a crosslinked actin filament network using an agent-based model. The link between these methods was given by the fact that each of them drew upon the output of the one at the smaller scale, by applying a bottom-up approach.

Atomistic level: molecular dynamics simulations

11 configurations of the actin monomer were defined, varying in terms of the bound nucleotide and nucleotide/cation(s): ATP-G-actin, ADP-G-actin, ADP-Pi-G-actin, ATP-1Mg^{2+}-G-actin, ATP-1Ca^{2+}-G-actin, ATP-6Mg^{2+}-G-actin, ATP-6Ca^{2+}-G-actin, ADP-1Mg^{2+}-G-actin, ADP-1Ca^{2+}-G-actin, ADP-6Mg^{2+}-G-actin, ADP-6Ca^{2+}-G-actin. The atomic coordinates of G-actin were obtained from the X-ray fiber diffraction structure reported in the RCSB protein data bank, 2zwh.pdb (Oda et al. 2009). The DB loop in the ADP-G-actin configurations was reconstructed using the atomic coordinates from 1j6z.pdb (Otterbein et al. 2001), by superimposition, in order to reproduce the folded configuration of this region in the ADP-state. Positions of six calcium, Ca^{2+} (or magnesium, Mg^{2+}) ions were taken from the crystallographic coordinates of 1j6z.pdb (Otterbein et al. 2001) (Fig. 1a). Atomic coordinates for ATP were taken from X-ray crystallography structure 1atn.pdb (Kabsch et al. 1990), after structural fitting. The monomer

subunits were arranged according to the microfilament model from (Grudinin and Redon 2010), as in (Deriu et al. 2012) (Fig. 1b). A repeat-unit of F-actin was placed in a rectangular box of 13 nm × 13nm × 37.5nm (Fig. 1c), with long axis parallel to z. Periodic boundary conditions were activated on xyz (Fig. 1d), maintaining along x and y a distance between the filament and its periodic images of at least 2 nm. The SPC model was used to simulate water molecules in the box. 5000 steps of energy minimization were applied using the steepest descent algorithm and a position restrain MD of about 50 ps was performed in isothermal-isobaric ensemble with the protein backbone restrained by a force constant of 1000 kJ mol^{-1} nm^{-2}. The NVT simulations were performed in a NVT ensamble at 300 K for 12 ns, as in (Deriu et al. 2012). All simulations were carried out with GROMACS 4 (Hess et al. 2008) using the G53a6 force-field (Oostenbrink et al. 2005). Electrostatic interactions were calculated with the Particle-Mesh Ewald method with a short-range electrostatic interaction cut off of 1 nm. A cut-off of 1 nm was also applied to Lennard-Jones interactions. The virtual site approach together with the LINCS constraint solver (Hess et al. 1997) allowed us to use a time step of 4 fs for the MD.

The Visual Molecular Dynamics (VMD) (Humphrey et al. 1996) package was employed for visual inspection and dedicated tools were developed in MATLAB for quantitative structural analysis. The output of equilibrium MD was analyzed using four parameters: the filament diameter, the distance between centers of mass of functional subdomains of adjacent monomer subunits (both inter- and intra-strand distances), the width of the nucleotide binding cleft and the dihedral angle. Our definition of subdomains followed the four subdomain (SD1-4) description of (Chu and Voth 2006a) (Fig. 2a). Parameters were reported in terms of average value and standard deviation between the 13 monomers of F-actin, giving a measure of the degree of heterogeneity of each configuration. We quantified how "closed" the nucleotide cleft was in two different ways: (1) by computing the distances between the centers of mass of the protein backbone of residues 57-69, 30-33 in SD2 and 203-216 in SD4 (Wriggers and Schulten 1997); (2) by measuring the distance between the mass centers of SD2 and SD4 (Splettstoesser et al. 2009; Düttmann et al. 2012).

Filament level: elastic network-based normal mode analysis

We used the 13-monomers repeat unit of F-actin from the MD output configurations (at 12 nm) to build filaments of 150 nm length, using rigid translations along z. The atomic model of each filament was then replaced by an Elastic Network Model (ENM) (Atilgan et al. 2001; Chennubhotla et al. 2005; Yang and Chng 2008), composed of nodes (points with a mass, identified by the protein Cα atoms) and springs. Nodes were connected by harmonic potentials of 1 kcal/molA^2, if closer than a cut-off distance of 1.2 nm (Doruker et al. 2000; Atilgan et al. 2001) (Fig. 1e). We applied the Rotation Translation Block (RTB) method (Philippe Durand et al., 1994; Tama et al., 2005; Tama et al., 2000; Tama et al., 2001). Blocks were defined based on the functional subdivision of each actin monomer into four subdomains, in order to preserve the basic topology of the actin subunit at the filament level (Fig.1f). This approach was considered since the filament has ~20000 Cα's and slow dynamics, with low frequency modes (around 10^{-1} cm) of interest. Also, since shear effects are negligible for an actin filament in deflection, we treated it as a homogenous and isotropic rod. From the frequencies associated with specific modes, the bending and extensional rigidities of F-actin were computed, as described in Supplementary Information.

Network level: Brownian dynamics simulations

We imported the bending and extensional rigidities of F-actin calculated by RTB under the different cation/nucleotide bound states into the agent-based model of a crosslinked actin network as input (Fig. 1g). Details about the network model can be found in our previous studies (Kim et al. 2009a; Kim 2014) and in Supplementary Information. Briefly, the model consists of F-actin and actin crosslinking proteins (ACPs). F-actin is modeled as a series of cylindrical segments of 140 nm in length and 7 nm in diameter, connected by elastic hinges. Harmonic potentials with extensional stiffness, k_s, and bending stiffness, k_f, obtained from RTB maintain the equilibrium length of actin cylindrical segments and keep the adjacent segments aligned in parallel, respectively. ACPs comprise two cylindrical segments of 23.5 nm in length and 10 nm in diameter connected serially by elastic hinges, forming permanent crosslinks between pairs of F-actins without preference of crosslinking angle by binding to sites located every 7 nm on the actin segment. We used two different values for extensional stiffness of ACPs, $k_{s,ACP} = 2\times10^{-3}$ (compliant) or 0.2 N/m (rigid), to maintain the equilibrium length of ACP segments. Bending stiffnesses of ACPs, $k_{f,ACP1} = 1.45\times10^{-25}$ Nm^2 and $k_{f,ACP2} = 5.8\times10^{-25}$ Nm^2 keep two ACP segments aligned in parallel and maintain an angle formed by an ACP segment and F-actin close to the right angle, respectively. Displacements of the actin and ACP segments are governed by the Langevin equation with stochastic forces, drag forces, and deterministic forces including the bending and extensional forces as well as repulsive forces between the actin segments accounting for volume-exclusion effects. Within a cubical computational domain whose width is 3 μm, actin and ACP segments in a monomeric state interact with each other by defined potential energies with a periodic boundary condition in all directions. It leads to the formation of a network whose average filament length is 1.2 μm, actin concentration is 20 μM, and relative density of ACPs (R_{ACP}) is 0.01. Then, F-actins passing through the boundaries in z direction (Fig. 1d) are severed and permanently clamped with the periodic boundary condition deactivated. To simulate a strain-stiffening behavior, the domain is subjected to shear deformation by translocating the top z boundary with a constant rate (0.1 s^{-1}) while the bottom z boundary is fixed (Fig.1h). Stress is calculated by dividing the sum of forces acting on the clamped filaments by area of the z boundary. The strain-stiffening behavior of the crosslinked actin networks was compared between cases with various combinations of nucleotide and cation(s).

RESULTS

Saturation of cation binding affects inter- and intra-strand F-actin interactions

Both inter- and intra-strand interactions between subdomains varied with a bound nucleotide or nucleotide/cation(s), especially for ADP-6Mg^{2+}-F-actins, corresponding to the physiological condition of F-actin in contractile muscle cells (Estes et al. 1992a). A schematic representation of a 3-monomers F-actin with coarse-grained subunits is shown in Fig. 2a, where each node corresponds to the mass center of one subdomain.

Repositioning of the mass centers of the subunit subdomains lead to a reduction of F-actin diameter of about 15 %, in both ADP- and ATP-F-actin (values reported in Supplementary Table 1). Saturation of Mg^{2+} at low- and intermediate-affinity binding sites enhanced this reduction (Fig. 2b), due to the repositioning of SD1 relative to SD1 of monomers *i* and *i+1* (Fig. 2c). This effect is consistent with the role that bound cations have in increasing the rigidity of SD1, which causes its shift (Nyitrai 1999).

A stabilizing effect was observed with cation saturation: mean values and standard deviations of distances between mass centers of subdomains were generally smaller than those of the corresponding cation-free and single-cation-bound F-actins. This effect was more marked in ADP-F-actin (Fig. 2c, d and e), and occurred in ATP-F-actin for the inter-strand distance between SD1 and SD1 (Fig. 2c) and for the intra-strand distance between SD2 and SD1 (Fig. 2e). It is conceivable that this effect is a consequence of reduced repulsions between subunits due to an increased number of bound cations (Janmey 1996; Kwon et al. 2005; Shi et al. 2007). In ATP-F-actin, intra-stand distances were also more heterogeneous with a single bound cation of either type (Fig. 2e), but inter-strand distances were more heterogeneous only with tightly bound Ca^{2+}(Fig. 2c and d). This effect can be related to the weaker coupling of Mg^{2+} with ATP, compared to that of Ca^{2+} (Nyitrai 1999).

At the end of the simulation period, the mass centers of SD2 and SD1 of subunits located in the same strand (monomers *i* and *i+2*) were closer by 3.3% in ATP-F-actins and 4.8% in ADP-F-actin (Fig. 2e), reflecting the unfolded or folded DB-loop's in ATP- and ADP-F-actin, respectively. In the case of the intermediate ADP-Pi-F-actin, the spacing within a filament was heterogeneous in the center of mass distances between SD2 and SD1 of adjacent longitudinal subunits (Fig. 2e), while distances between opposite SD1/SD1 and SD4/SD1 were more uniform (Fig. 2c and d). Unbinding of the γ–phosphate from the nucleotide leads to F-actin compaction along its diameter (Fig. 2b) without heterogeneous coupling between longitudinal monomers (Fig. 2e).

Cation saturation increases variability in dihedral angle and nucleotide cleft size

The dihedral angle (indicated by an arrow in Fig. 3a) decreased in the range 0.7-1.4% for ATP-, ADP- and ADP-Pi- filaments (Fig. 3b). Estimates of the average dihedral angle for each F-actin are listed in Supplementary Table 1.

The binding of either Ca^{2+} or Mg^{2+} to the low- and intermediate-affinity sites of both ATP and ADP filaments increased the variance of the dihedral angle with respect to the corresponding configurations with only the high-affinity site occupied (Fig. 3b). This effect is opposite to that of the cations on the inter- and intra- strand subunit interactions: saturation of cation binding sites made ADP-F-actin more uniform in intra- and inter-strand monomer subunit interactions (Fig. 2c, d, and e). This result suggests that cation saturation may induce stabilization of inter and intra-subunit interactions while allowing heterogeneous repositioning of the two major subdomains of the monomer subunit (the largest one including SD1 and SD2, the smallest one including SD3 and SD4) along the filament. This result is in agreement with the observed effect of multiple cations in reducing electrostatic repulsions between subunits (Janmey 1996; Kwon et al. 2005; Shi et al. 2007).

Interactions of low- and intermediate-affinity cations were weaker than those of the high-affinity cations (Fig. 3c) and the amplitude of cation fluctuations was independent of the type of bound nucleotide (Fig.S1). However, the type of bound cation had a direct effect on the dimension of the cleft between the two major domains of the subunit (Fig. 3d and e). A detailed comparison between cleft openings in systems with ADP, ATP and ADP-Pi can be found in the Supplementary Information. Fig 3d-e show that after release of Pi, the cleft is more stable in an open conformation, consistent with previous MD simulations (Pfaendtner et al. 2009). The presence of only the tightly bound cation, either Ca^{2+} or Mg^{2+}, in ADP-F-actin, lead to an increase of the cleft opening relative to the cation-free F-actin, and if saturation of all cation

binding sites occurred, this opening was more accentuated (Fig. 3e). By contrast, in ATP-F-actin, the cleft was greater only with saturation of Ca^{2+} (Fig. 3e).

Binding of nucleotide/cation(s) minimally impact the extensional and bending rigidities of F-actin

In both ATP- and ADP-bound forms, Mg^{2+}-F-actin was less rigid than Ca^{2+}-F-actin if only the high-affinity cation binding site was occupied, (Fig. 4). For ADP-F-actin, bending rigidity was also slightly reduced when the low- and intermediate-affinity binding sites were occupied. An opposite effect was observed with the binding of multiple cations on ATP-F-actin, where the Mg^{2+}-F-actin was more rigid in bending than Ca^{2+}-F-actin. Cation saturation in Mg^{2+}-ATP-F-actin also led to enhanced variability in inter-strand distances between SD4/SD1 (Fig. 2d).

The variation in extensional rigidity between the different nucleotide and nucleotide/ cation(s) bound forms reflected changes in bending rigidity, except for Ca^{2+} saturation, where ADP-F-actin was more rigid in extension than ATP-F-actin (Fig. 4a). Values for flexural and extensional rigidities of each system are given in Supplementary Table 3.

The variance of the root mean square distance of the monomer subunits α-carbons from the average structure in each conditions of bound nucleotide and nucleotide/cation(s) mirrors differences in filament persistence length (Fig.4c). Therefore, increased anisotropy corresponds to increased F-actin rigidity.

Cation binding at low-, intermediate-, and high-affinity sites can affect strain-stiffening of a crosslinked actin network depending on crosslinker stiffness

Values of bending and extensional stiffnesses of F-actin calculated under different nucleotide and cation binding using RTB were imported to k_s and k_f in our model for crosslinked actin networks. We compared the strain-stiffening behavior between 11 cases with various k_s and k_f using either soft or rigid ACPs. In all the sampled cases, we observe a tendency that shear stress increases in direct proportion to shear strain below ~0.5 strain while stress rapidly diverges above the critical strain, determining the onset of nonlinear stiffening (Fig. 5a, b, c, d). As shown in Fig.5a, with soft ACPs, the strain-stiffening curves of the 11 cases did not show statistically significant differences (average p-value = 0.88, with 95% confidence). This is because k_s corresponding to all values of l_p was much higher than $k_{s,ACP}$ which mimics the mechanical properties of filamin A and α-actinin (Golji et al. 2009). In other words, the actin cylindrical segments connected in F-actin with very high k_s would behave like rigid rods, whereas the ACPs connecting the actin segments would act as soft spring. Then, since the network-level response will be dominated by mechanical response of the ACPs, a change in k_s will lead to the minimal alteration in the strain-stiffening behavior as we observed. By contrast, with stiff ACPs, strain-stiffening curves were statistically different (average p-value = 0.03, with 95% confidence) (Fig.5b). Although any of our sampled cases with binding of low-, intermediate- and high-affinity cations in various nucleotide states did not substantially affect the strain-stiffening behavior with soft ACPs, it is still possible that binding of cations at a different site can lead to significant changes in the network rheology. Thus, we extended our scope by incorporating a large increase in l_p which results from discrete binding of Mg^{2+} to the so-called "stiffness" site identified by a combination of microscopic techniques with image analysis approaches (Kang et al. 2012). They found that l_p is elevated from 2.1 to 12.7 μm when concentration of $MgCl_2$ is increased from 0.5 to 5 mM. We estimated values of k_s and k_f from the measured l_p with assumption of an ideal polymer chain and elastic rod theory, and incorporated them into our

network model. We observed a statistically significant difference between strain-stiffening curves even with soft ACPs (average p-value < 0.01) (Fig.5c); the largest difference the curves was about 25% at high strains. This effect was highly magnified with stiffer ACPs; stress with the highest l_p was 3-fold greater than that with the lowest l_p (Fig. 5d). Differences in network elasticity at high strains are illustrated in Fig. 5e (soft ACP) and Fig. 5f (rigid ACP).

DISCUSSION AND CONCLUSIONS

In this study, we used a multiscale computational approach in order to investigate the effect of the molecular conformation of F-actin on filament rigidity and on the elasticity of a crosslinked actin network. We used as case study models of F-actin bound to a nucleotide (ATP, ADP or ADP-Pi) in combination with one or multiple cations (Ca^{2+}, Mg^{2+}). We first employed MD simulations and RTB analysis to compute F-actin rigidity. Then, we incorporated the results into our model of crosslinked actin network. This study is novel in that it presents the first combination of computational techniques addressing the conformational and mechanical properties of the actin structure from the molecular rearrangement of monomer subunits in F-actins up to strain-induced stiffening of a network composed of numerous F-actin filaments. Advantages of this computational approach arise from passing information from one level of modeling to the other, thus enabling us to study the actin structures at multiple temporal and spatial scales.

Different monomer conformations varying for bound nucleotide and nucleotide/cation(s) resulted in different intra-strand (longitudinal contacts) and inter-strand (lateral contacts) distances between subdomains along the same filament, which affected the dihedral angle per subunit, and conversely, changes in the dihedral angle of subunits induced different inter- and intra-strand distances between subdomains. In ADP-F-actin, saturation of binding sites led (1) to a reduction in heterogeneity of the inter- and intra- subdomain distances and (2) to an increased heterogeneity in the dihedral angles (Fig. 3a, b). On the contrary, for ATP-bound filaments, with either one or multiple cations, inter- and intra-strand subunit distances were always observed to be heterogeneous among the 13 monomer subunits in the filament model. This gave rise to filaments more rigid in bending (up to 12% stiffer) compared to the analogous systems in the ADP-bound form, consistent with experimental results (Gittes et al. 1993; Ott et al. 1993; Kojima et al. 1994; Isambert et al. 1995; Belmont et al. 1999) as well as computational characterizations (Chu and Voth 2005; Splettstoesser et al. 2009), reporting changes in rigidity of about 24% (Isambert et al. 1995) and 16-45% (Chu and Voth 2006b), respectively. Overall, variations in the Cα positions per actin subunit resulting from MD led to heterogeneities along the filaments which mirror the changes in rigidity (Fig 4a, c). We compared our MD-refined subunits with Oda's, Fujii's, and Murakami's models of actin (Fig.S2), which were obtained in different solutions conditions, Ca^{2+}-ADP, Mg^{2+}-ADP and Mg^{2+}-ADP Pi, respectively. Among the tested actin configurations, the monomer subunit closest to the Murakami's model (Murakami et al. 2010) at the output of MD was ADP-Pi-G-actin (RMSD 3.6 Å, see Table S5). Our Ca^{2+}-ADP- subunits had smaller RMSD of Cα atoms (4.03 or 3.60 Å) from the Oda's model (Oda et al. 2009) than from the Fujii's (Fujii et al. 2010) or Murakami's models (RMSD > 4.09 or 3.91 Å, see Table S5). Similarly, our Mg^{2+}-ADP- subunits showed smaller RMSD of Cα atoms (3.25 or 3.89 Å) from the Fujii's model than from the Oda's or Murakami's models (RMSD > 3.83 or 4.04 Å, see Table S5). These results are consistent with the different solution conditions used to obtain the above mentioned actin models. In addition, the smallest RMSD of

Cα pertaining to SD2 corresponded to that of Mg^{2+}-ADP- subunit from the Fujii's model (see Table S4), owing to the replacement of SD2 in 2zwh.pdb. The binding of the sole high-affinity Ca^{2+} resulted able to keep the monomer in its flat configuration in ATP-F-actin, whereas if Mg^{2+} was tightly bound to ATP-F-actin, the dihedral angle was reduced (Fig. 3b). This unflattened configuration may be related to the faster polymerization rate observed in ATP-F-actin tightly bound to Mg^{2+} (Selden et al. 1983). When the transition from ATP-Pi-F-actin to ADP-F-actin occurred in the presence of tightly bound Mg^{2+} the configuration of the subunit returned to the flattened state (increase in dihedral angle), which is the form of the monomer subunit in a double-stranded helix (Oda et al. 2009). Our findings suggest that for monomer subunits saturated with cations, the opening of the nucleotide cleft due to hydrolysis leads to a reduction in the subunit average dihedral angles (Fig. 2b), and consequently to thinner ADP-F-actins with decreased rigidity (Fig. 4a).

In general, saturation of cation binding sites induced a change in the persistence length of F-actin from 3.5 to 4 μm, depending on the nucleotide and nucleotide/cation(s) (Fig.4). Recent experimental data have shown that specific cation binding to the actin filament can be related to changes in its bending rigidity from about 3 to 12 μm, depending upon the Ca^{2+} or Mg^{2+} concentration in the solution and the site of binding (Kang et al. 2012). Our results indicate values of persistence length at the lower end of this range, since none of the cations here used is bound to the so-called "stiffness" site detected in (Kang et al. 2012) and responsible for pronounced changes in filament rigidity. Earlier studies have shown that bending rigidity of Mg^{2+}-F-actin is about four times lower than Ca^{2+} actin (Orlova and Egelman 1995). However, spectroscopic experiments showed that Ca^{2+}-F-actin are less rigid in bending that Mg^{2+}-F-actin (Hild et al. 1998). Also, other studies found essentially no cation dependence of the flexibility of filaments using either dynamic light scattering measurements (Scharf and Newman 1995), or other techniques (Isambert et al. 1995; Steinmetz et al. 1997) to determine F-actin persistence length. Our results corroborate these last studies and together with the evidences from (Kang et al. 2012) support that precise location of cation binding, different from low-, intermediate- and high-affinity sites, can be responsible for the pronounced changes in F-actin rigidity detected in (Kang et al. 2012).

Existence of cations at low-, intermediate-, and high-affinity sites used in the present study minimally influenced F-actin stiffness and did not significantly affect strain-stiffening of networks with soft ACPs that mimic filamin A and α-actinin. It is expected that overall stiffness of a network consisting of rigid and soft elements is determined largely by the soft elements which are the crosslinkers in this case, and then the network stiffness would be insensitive to slight changes in the rigidity of the stiff elements which are the actin filaments. However, the same cation binding markedly varied network strain-stiffening when ACPs are as stiff as actin filaments, like scruin, since the contribution of actin filaments to the network stiffness becomes significant under this condition. In our previous work (Kim et al. 2009b), storage shear modulus, *G*', of a crosslinked actin network showed a noticeable change in response to a 25-fold decrease in the extensional and bending stiffness of actin filaments because we used extensional stiffness of actin filaments that is only 4-fold greater than that of compliant ACPs in order to decrease computational costs. Bending stiffness of actin filaments was set to be smaller than that of ACPs. This is consistent with our current results in that the strain-stiffening is highly influenced by a change in actin-filament rigidity only when actin filaments and ACPs have comparable rigidity. Furthermore, using the values of F-actin persistence length reported in (Kang et al. 2012)

originating from Mg^{2+} binding to the monomer "stiffness" site made strain-stiffening curves of the crosslinked actin networks statistically different even with soft ACPs.

Based on this finding, we conclude that: (1) alterations in F-actin rigidity induced by binding of one or multiple cations at the low-, intermediate-, or high-affinity sites can impact the strain-stiffening of actin networks depending on whether ACPs are stiff or compliant; (2) binding of cations at specific "stiffening" locations between adjacent subunits is reflected not only at the filament level (Kang et al. 2012), but also at the network level regardless of rigidity of ACPs. In the context of cell mechanics, our overall results suggest that the binding of one or multiple cations in the different nucleotide-bound forms of F-actin should be considered as a potential mechanism for cell's ability to modulate the mechanical properties of the cytoskeleton crosslinked by very rigid ACPs.

Numerous computational studies have shown that F-actin bending is important at low shear strain, whereas extension plays a significant role at high shear strain (Head et al. 2003; Onck et al. 2005; Broedersz and Mackintosh 2014). Considering that most ACPs form reversible crosslinks which lead to the collapse of stress during strain-stiffening before reaching high strains (Wagner et al. 2006; Gardel et al. 2006c; Kim et al. 2011), the change in extensional stiffness induced by the cation binding might be less important for rheology of cells than that in bending stiffness. In addition, although the cation binding shows a negligible effect on network rheology with compliant ACPs at concentration and length of F-actin tested here, it still has potential to result in high impact on network elasticity at regimes where actin concentration and filament length are significantly different due to actin dynamics regulated by various proteins and/or molecules. For example, regarding Mg^{2+} or Ca^{2+} binding, previous studies demonstrated that Mg^{2+}-ATP-actin polymerizes about two times faster than Ca^{2+}-ATP-actin (Selden et al. 1983; Carlier et al. 1986; Estes et al. 1987; Estes et al. 1992a), and the resulting increased filament length can induce differences in network rheology between Mg^{2+} and Ca^{2+}-networks even with compliant ACPs. As a focus for future work, studies of cation binding within the SD2 domain may reveal larger changes in stiffness than those observed in our study. Also, incorporation of torsional rigidity into the actin network model and characterization of the bending-torsional coupling relative to strain-stiffening behavior may reveal differences in network elasticity brought by low-, intermediate-, and high-affinity cation binding.

ACKNOWLEDGMENTS

We gratefully acknowledge a fellowship from the MITOR program to TCB.

SUPPLEMENTARY INFORMATION

Extracting mechanical properties of the actin filaments from Normal Mode Analysis

Normal Mode Analysis (NMA) is a powerful approach for analyzing the structural and dynamical features of macromolecules such as actin filaments (Tirion 1996; Bahar and Rader 2005; Hinsen 2005; Dykeman and Sankey 2010). Although it is approximate because only the harmonic motions of the system around a single potential minimum is considered, the low frequency normal modes can be directly related to the mechanical behavior of the protein under the assumption of homogenous and isotropic material (Flynn and Ma 2004; Park et al. 2006; Adamovic et al. 2008). In our study, we first represent the filament structure as a network of Cα atoms locally connected by springs. Then, we ignore local flexibilities of selected groups of Cα by defining rigid blocks and applying an approximation of the NMA method in order to extract the mechanical properties of F-actin, Rotation Translation Block (RTB) approach. Before describing how the RTB method approximates NMA analysis, we provide here in the following some details about NMA. We will illustrate how mechanical properties can be related to frequencies of vibration associated with specific modes of motion of the actin filament, thought NMA.

Considering F-actin as a linear elastic material, its mechanical behavior can be related to its status of deformation and characterized by: stiffness in bending, also called flexural rigidity k_f; and stiffness in elongation, k_s. For small deformations, the components of displacement, expressed as functions of axial coordinate (e.g., z) and time t, satisfy wave equations for both bending displacement $u_f(z,t)$ and stretching displacement $u_s(z,t)$:

$$\rho \frac{\partial^2 u_f(z,t)}{\partial t^2} = -k_f \frac{\partial^4 u_f(z,t)}{\partial z^4} \tag{S1}$$

$$\rho \frac{\partial^2 u_s(z,t)}{\partial t^2} = -k_s \frac{\partial^2 u_s(z,t)}{\partial z^2} \tag{S2}$$

where ρ is the mass per length unit of F-actin, of about 2.3 10^{-16} Kg/m and ρ_v is its mass per unit volume, of about 11.6 Kg/m^3. The general solution of Eqs. S1 and S2 are expressed as a linear combination of hyperbolic sinusoidal waves:

$$u_f(z,t) \approx \begin{pmatrix} \cos(w_n z) \\ \sin(w_n z) \\ \cosh(w_n z) \\ \sinh(w_n z) \end{pmatrix} e^{-i\omega_n t} \tag{S3}$$

$$u_s(z,t) \approx \begin{pmatrix} \sin(w_n z) \\ \cos(w_n z) \end{pmatrix} e^{-i\omega_n t} \tag{S4}$$

The last two systems of equations can be used to find the relation of dispersion between wave number w_n, and angular frequency ω_n (1/s) as:

$$\rho\omega_n^{\,2} = k_f\, w_n^{\,4} \tag{S5}$$

$$\rho\omega_n^{\,2} = k_s w_n^{\,2} \tag{S6}$$

Depending on the boundary conditions, linear combinations of the general solution (Eqs. 1 and 2) can be used. In the case of NMA, the filament is not clamped, so the correspondent boundary conditions, both in bending or stretching are $u'_{f,s}(0)=0$ and $u''_{f,s}(L)=0$, where L is the length of the filament.

Considering the bending modes, the corresponding solution for a filament free to vibrate in a three dimensional space is given by:

$$u_f(z,t) = \sum_n a_n \left\{ -\left[\cos(w_n z) + \cosh(w_n z)\right] - \left(\frac{\cos(w_n z) - \cosh(w_n z)}{\sin(w_n z) - \sinh(w_n z)} \right) \left[\sin(w_n z) + \sinh(w_n z)\right] \right\} e^{-i\omega_n t} \tag{S7}$$

with wave number w_n given by the relation:

$$\cos(w_n L) + \cosh(w_n L) = 1 \tag{S8}$$

With negligible viscous drag, the amplitude a_n of the n^{th} mode is determined by the initial conformation of the filament.

Considering the stretching modes, the corresponding solution is given by:

$$u_s(z,t) = \sum_n a_n \cos(w_n z)\; e^{-i\omega_n\, t} \tag{S9}$$

with wave number w_n for the n^{th} mode given by:

$$w_n = \frac{n\pi}{L} \tag{S10}$$

Once extracted the normal modes and the related frequencies, the mechanical proprieties are calculated by applying linear elastic beam theory.

A linear elastic beam has constant stiffness when bending, k_f, or stretching, k_s. This constant stiffness is related to the eigenvalue of the correspondent modes of motion as follows.

The bending modulus Y_f is calculated as:

$$Y_f = \frac{k_f}{I} \tag{S11}$$

Under the assumption of an isotropic and homogenous material, the bending modulus is equal to the Young's modulus. The stretching modulus Y_x, i.e. the Young's modulus, is calculated directly by the stretching modes:

$$Y_x = \frac{k_s}{A} L \tag{S12}$$

where k_s is the extensional stiffness, A is the cross-sectional area of the filament (~ 19.6 nm^2). The persistence length l_p, is related to the bending stiffness k_f, the Boltzmann constant k_B, and the temperature T, through:

$$l_p = \frac{k_f}{k_B T} \tag{S13}$$

Using Rotation Translation Block approach to approximate NMA

The Rotation Translation Block (RTB) approach is an approximation of the NMA and reproduces the lowest-frequency modes of motion of the system with reasonable accuracy at low computational cost. This renders this approach particularly suitable when dealing with large systems, as the actin filaments here considered, composed by about 20000 Cα.

Using the Rotation Translation Block (RTB) approach, the molecular system is divided in n_b rigid blocks, with each block made of a certain number of C_α-atoms. For the actin filament, we used the functional subdivision of each monomer subunit along the filament in four subdomains. We consider each block as a rigid body, neglecting internal flexibilities within each actin subdomain. Deformation of the whole actin filament are given by rotation-translation movements of the rigid blocks (Durand et al. 1994; Tama et al. 2000).

With the rotation translation block approach, the full hessian matrix, **H**, is expressed in a basis, $\mathbf{H_b}$, defined by rotations and translations of the n_b rigid blocks:

$$\mathbf{H}_b = \mathbf{P}^T \mathbf{H} \mathbf{P} \tag{S14}$$

where **P** is an orthogonal $3N$ x $6n_b$ matrix, built with the vector associated to the local rotations/translations of each block. Approximate low-frequency normal modes are calculated by diagonalizing $\mathbf{H_b}$, which is a reduced matrix of size $6n_b$ x $6n_b$, instead of the entire original matrix **H** of size $3N$ x $3N$, where N is the number of C_α-atoms in the system.

The corresponding atomic displacements of all C_α-atoms of the system are given by:

$$\mathbf{A}_p = \mathbf{P}\mathbf{A}_b \tag{S15}$$

where $\mathbf{A}_b$ is the matrix of the eigenvectors of $\mathbf{H_b}$.

The eigenvectors can be expanded back to the atomic space using the transpose of the projector **P**.

Brownian Dynamics simulations of a crosslinked actin filament network

In the network model, actin filaments are modeled as semiflexible polymers represented by a series of cylindrical segments connected by elastic hinges, and actin crosslinking proteins (ACPs) are modeled as a pair of cylindrical segments connected by elastic hinges (Fig.1g). Harmonic potentials describe the extension and bending of both ACPs and actin filaments:

$$U_s = \frac{1}{2} k_s \left(r - r_0 \right)^2 \tag{S16}$$

$$U_b = \frac{1}{2} k_b \left(\theta - \theta_0 \right)^2 \tag{S17}$$

where k_s is extensional stiffness, r is an instantaneous distance, r_0 is an equilibrium length, k_b is bending stiffness, θ is an instantaneous bending angle, and θ_0 is an equilibrium bending angle ($r_{0,A}$ = 140 nm, $r_{0,ACP}$ = 23.5 nm, $\theta_{0,A}$ = 0 rad, $\theta_{0,ACP1}$ = 0 rad, $\theta_{0,ACP2}$ = π/2 rad). Langevin equation governs displacements of segments for actin and ACPs, with inertia neglected:

$$\mathbf{F}_i - \zeta_i \frac{d\mathbf{r}_i}{dt} + \mathbf{F}_i^T = 0 \tag{S18}$$

where $\mathbf{r}_i$ is the position vector for either the center of ACP or the endpoint of the actin segment, ζ_i is an effective drag coefficient, t is time, $\mathbf{F}_i^T$ is a stochastic force, and $\mathbf{F}_i$ is a net deterministic force. For the cylindrical geometry of the segments for actin filaments and ACPs, the effective drag coefficient is defined as (Clift et al. 2005):

$$\zeta_i = 3\pi\mu r_{c,i} \frac{3 + 2r_{0,i} / r_{c,i}}{5} \tag{S19}$$

where $r_{c,A}$ = 7 nm and $r_{c,ACP}$ = 10 nm are diameter of the actin and ACP segments, respectively, and μ = 0.086 Pa·s is the viscosity of surrounding medium. The thermal force $\mathbf{F}_i^T$ obeys the fluctuation-dissipation theorem:

$$\left\langle \mathbf{F}_i^T(t) \cdot \mathbf{F}_j^T(t) \right\rangle = \frac{2k_B T \zeta_i \delta_{ij}}{\Delta t} \boldsymbol{\delta} \tag{S20}$$

where δ_{ij} is the Kronecker delta, $\boldsymbol{\delta}$ is a unit second-order tensor, and $\Delta t = 2.31 \times 10^{-8}$ s is a time step. Repulsive forces between actin cylindrical segments are computed using a minimal distance between the segments, r_{12}, and the following harmonic potential:

$$U_r = \begin{cases} \frac{1}{2} k_r \left(r_{12} - r_{c,A} \right)^2 & \text{if } r_{12} < r_{c,A} \\ 0 & \text{otherwise} \end{cases} \quad \text{(S21)}$$

where $k_r = 1.69 \times 10^{-3}$ N/m is the strength of repulsive effects. Positions of the segments over time are updated using the Euler integration scheme:

$$\mathbf{r}_i(t + \Delta t) = \mathbf{r}_i(t) + \frac{d\mathbf{r}_i}{dt} \Delta t = \mathbf{r}_i(t) + \frac{1}{\zeta_i} \left(\mathbf{F}_i + \mathbf{F}_i^T \right) \Delta t \quad \text{(S22)}$$

Comparison in inter- and intra-subunit mass center distances and residue fluctuations between different nucleotide bound F-actins

All simulation results are computed from the filament structure at 12 ns of equilibrium MD simulations with respect to the corresponding structures used as input for the simulations; values are averaged over the 13 monomers of the filament repeat unit.

The inter-strand distance between SD4 and SD1 was reduced by 9.40% in both nucleotide-bound forms of F-actin (Fig. 2d), representing a reduction in filament diameter. In particular, the SD1 domains of opposite monomers (monomers *i* and *i+1*) were 5.85% closer in ATP-F-actin and 6.54 % closer in ADP-F-actin (Fig. 2c), showing that the opening of the nucleotide binding cleft due to ATP hydrolysis did not prevent opposite subunits from coming closer together.

The average distance between SD4 and SD3 of adjacent subunits in opposite strands (monomers *i* and *i+1*) increased 1.43% in ATP-F-actin, while it did not change in ADP-F-actin. It is possible that the opening of the cleft in ADP-F-actin causes steric hindrance that prevents the increase of contact between these two subdomains.

Molecular rearrangements of the nucleotide resulted in slightly higher RMS fluctuations for ADP than ATP. Considering all filaments but the ADP-Pi system, RMS fluctuations of ADP and ATP were 1.586 ± 0.006 Å and 1.527 ± 0.006 Å, respectively, relative to the subunit configurations at the onset of MD simulations. Cleavage of the γ-phosphate from ATP to create the ADP-Pi intermediate form of the monomer subunit destabilized the nucleotide up to average RMS fluctuations of 2.361 ± 0.967 Å, confirming that this is an intermediate form of the system. Values of RMS fluctuations at equilibrium for selected regions of the monomer subunits in all systems are reported in Supplementary Table 2.

The DB loop (residues 38-52) showed the highest fluctuations among the residues of the monomer subunits. It was more mobile in ATP filaments (with RMS fluctuations of 2.5 ± 0.063 Å) than in ADP filaments (with RMS fluctuations of 2.112±0.114 Å), reflecting its different conformations (disordered in ATP-bound monomers and helical in ADP-bound monomers). This result is in agreement with the higher SD1-SD2 distances found for the ATP systems with respect to the ADP-bound systems (Fig. 2e). The hydrophobic loop (HL loop, including residues 262-274) to which the DB loop binds between adjacent intra-strand subunits did not show discernible differences in terms of RMS fluctuations between the various systems, and presented an average value of 1.58 ± 0.08 Å. In SD1 of all filaments, the C-terminus (residues 370-375) was slightly more mobile than the N-terminus (residues 1-21).

C- and N-termini did not show discernible differences in RMS fluctuations between the three nucleotide systems. In the ATP-filaments, the RMS fluctuations of the C- and N-termini were 1.93 ± 0.09 Å and 1.52 ± 0.02 Å, respectively. In the ADP filaments the RMS fluctuations of the C- and N-termini were 1.86 ± 0.04 Å and 1.62 ± 0.04 Å, respectively. In the ADP-Pi filament form, the C- and N-termini had RMS fluctuations of 1.96 ± 0.04 Å and 1.58 ± 0.04 Å, respectively.

For ADP-bound filaments, the increase of the mass center distances between SD2 and SD4 was 5.37% and the increase in cleft size was 19.36%; for ATP- bound filaments, the increase of the distance between the mass centers of SD2 and SD4 was 3.96% and the increase in cleft size was 12.85%. Our data agree with previous results documenting the opening of the nucleotide binding cleft upon nucleotide hydrolysis, and also show that the increase of the space between the two subdomains is due to both major repositioning of SD2 with respect to SD4, and to an even greater extent, rearrangements of internal residues between the two subdomains. These residues, used to compute the cleft size, interact directly with the nucleotide. Furthermore, comparing

ADP-Pi-F-actin with the initial ADP-F-actin configuration, the average cleft was larger by 6.14% and 16.19%, in terms of distance between the mass centers of SD2 and SD4 and in terms of cleft size, respectively. These results support that at equilibrium ATP filaments have a narrower nucleotide cleft than ADP filaments. This result is in agreement with experimental observation documenting that assembled actin monomers favor a closed cleft in the ATP and ADP-Pi states, owing to the strong contact between the nucleotide's P_β atom and the protein backbone, and an open configuration in the ADP state, where the protein loses its contacts with the phosphate. Our results also show that from the release of the bond between nucleotide and γ-phosphate until complete dissociation of the γ-phosphate, most of the cleft opening already occurs during the intermediate ADP-Pi phase. This behavior reflects the variations here observed for the dihedral angle (**Error! Reference source not found.**b).

Supplementary Table 1. Structural properties of the nucleotide- and nucleotide/cation(s)-bound forms of F-actin related to the reorganization of F-actin

	Filament radius (Å)	Dihedral angle (°)
ADP-F-actin	41.8	173.8±2.5
ADP-1Mg-F-actin	40.5	174.3±3.2
ADP-6Mg-F-actin	37.3	172.1±5.4
ADP-1Ca-F-actin	40.1	174.1±3.1
ADP-6Ca-F-actin	38.9	172.5±4.7
ATP-F-actin	43.4	174.1±4.2
ATP-1Mg-F-actin	41.3	173.4±3.8
ATP-6Mg-F-actin	37.2	173.9±4.3
ATP-1Ca-F-actin	42.5	177.2±2.6
ATP-6Ca-F-actin	39.8	174.5±3.3
ADP-Pi-F-actin	40.1	173.6±3.9

669 **Supplementary Table 2.** Structural properties of the nucleotide- and nucleotide/cation(s)-bound
670 forms of F-actin related to the reorganization of selected regions within monomer subunits
671

	RMSD C_α (Å)	RMSD DB loop(Å)	RMSD C-term(Å)	RMSD N-term(Å)	RMSD HL (Å)	RMSD Cys374 (Å)	RMSD Gln41 (Å)
ADP-F-actin	4.77±2.47	4.92±1.44	5.98± 2,53	5.65±1.75	4.13±0.89	5.46±2.43	4.83±1.27
ADP-1Mg-F-actin	4.37±2.50	5.29± 2.22	5.55± 2.22	5.78±1.34	3.31±0.80	5.16±1.98	5.33±2.69
ADP-6Mg-F-actin	4.95± 2.62	5.98± 3.06	6.63± 1.45	7.17±1.68	3.43±0.97	6.85±1.59	5.49±2.88
ADP-1Ca-F-actin	4.34±2.47	5.58± 1.92	5.74± 2.62	5.79±1.49	3.29±1.06	5.54±2.67	4.67±2.16
ADP-6Ca-F-actin	5.01±2.66	7.08± 1.42	6.67± 2.80	6.35±1.48	3.39±0.81	6.31±2.85	5.84±1.89
ATP-F-actin	4.59± 2.51	5.78± 2.03	5.88± 1.49	5.67±1.65	3.64±0.97	5.50±1.94	4.79±1.95
ATP-1Mg-F-actin	4.72±2.66	6.99± 3.44	6.42± 2.63	6.15±2.08	4.13±1.61	5.93±2.76	7.32±3.22
ATP-6Mg-F-actin	4.51±2.37	5.04± 1.24	5.93± 1.61	5.39±1.58	3.88±1.55	5.32±2.42	4.45±1.62
ATP-1Ca-F-actin	4.34±2.39	4.88± 1.68	5.70± 1.89	5.35±1.55	4.39±1.65	5.37±1.82	4.90±1.88
ATP-6Ca-F-actin	4.85±2.73	6.59± 2.17	6.56± 1.74	6.37±2.15	3.45±1.15	5.81±1.97	5.13±1.59
ADP-Pi-F-actin	5.65± 2.87	5.99± 1.59	6.12± 1.55	6.63±2.29	4.65±1.51	5.64±1.92	5.56±2.43

672

673

Supplementary Table 3. Mechanical properties of the nucleotide- and nucleotide/cation(s)-bound forms of F-actin

	l_p [μm]	k_f [Nm^2]	k_s [N/m]
ADP-F-actin	3.92	1.63 E-26	6.93E-2
ADP-1Mg-F-actin	3.95	1.64 E-26	6.99 E-2
ADP-6Mg-F-actin	3.76	1.56 E-26	6.64 E-2
ADP-1Ca-F-actin	3.86	1.61 E-26	6.83 E-2
ADP-6Ca-F-actin	3.73	1.54 E-26	6.59 E-2
ATP-F-actin	4.01	1.66 E-26	7.08 E-2
ATP-1Mg-F-actin	3.83	1.58 E-26	6.76 E-2
ATP-6Mg-F-actin	3.65	1.51 E-26	6.45 E-2
ATP-1Ca-F-actin	3.76	1.56 E-26	6.65 E-2
ATP-6Ca-F-actin	4.02	1.66 E-26	7.10 E-2
ADP-Pi-F-actin	3.91	1.62 E-26	6.91E-2

Supplementary Table 4. Residues of actin domains and corresponding RMS displacements of their Cα atoms between our MD-refined subunits and models from Oda, Fujii and Murakami

Subdomain	Residues	1Mg-ADP-G-actin vs Fujii's	6Mg-ADP-G-actin vs Fujii's	1Ca-ADP-G-actin vs Oda's	6Ca-ADP-G-actin vs Oda's	ADP-Pi-G-actin vs Murakami's
1	1-32, 70-144, 338-375	3.56 Å	4.78 Å	4.10 Å	3.25 Å	3.34 Å
2	33-69	2.89 Å	3.62 Å	5.30 Å	6.15 Å	5.07 Å
3	145-180, 270-337	3.04 Å	3.15 Å	4.26 Å	2.62 Å	3.38 Å
4	181-269	3.34 Å	3.97 Å	2.42 Å	4.82 Å	3.71 Å
whole G-actin		3.25 Å	3.89 Å	4.03 Å	3.60 Å	3.60 Å
whole F-actin		4.03 Å	4.19 Å	3.66 Å	3.94 Å	3.91 Å

Supplementary Table 5. RMS deviations of Cα atoms between our MD-refined subunits and the corresponding actin models.

	Oda's	Fujii's	Murakami's
1Ca-ADP-G-actin	4.03 Å	4.23 Å	4.09 Å
6Ca-ADP-G-actin	3.60 Å	3.91 Å	4.04 Å
1Mg-ADP-G-actin	3.83 Å	3.25 Å	4.85 Å
6Mg-ADP-G-actin	4.04 Å	3.89 Å	4.06 Å
ADP-Pi-G-actin	3.69 Å	3.70 Å	3.60 Å

Supplementary Figure 1. Root Mean Square (RMS) fluctuations of cations. Intermediate- and low-affinity cations fluctuate more than high-affinity cations in all conditions of bound nucleotide.

Supplementary Figure 2. Comparison of our MD results with three actin models. (a-b) 1Mg-ADP-G-actin and 6Mg-ADP-G-actin (magenta) vs Fujii's. (c-d) 1Ca-ADP-G-actin and 6Ca-ADP-G-actin (magenta) vs Oda's. (e-f) ADP-Pi (magenta) vs Murakami's.

REFERENCES

Adamovic I, Mijailovich SM, Karplus M (2008) The elastic properties of the structurally characterized myosin II S2 subdomain: a molecular dynamics and normal mode analysis. Biophys J 94:3779–3789. doi: 10.1529/biophysj.107.122028

Atilgan AR, Durell SR, Jernigan RL, et al. (2001) Anisotropy of fluctuation dynamics of proteins with an elastic network model. Biophys J 80:505–515. doi: 10.1016/S0006-3495(01)76033-X

Bahar I, Rader AJ (2005) Coarse-grained normal mode analysis in structural biology. Curr Opin Struct Biol 15:586–592. doi: 10.1016/j.sbi.2005.08.007

Bausch AR, Möller W, Sackmann E (1999) Measurement of local viscoelasticity and forces in living cells by magnetic tweezers. Biophys J 76:573–579. doi: 10.1016/S0006-3495(99)77225-5

Belmont LD, Orlova A, Drubin DG, Egelman EH (1999) A change in actin conformation associated with filament instability after Pi release. Proc Natl Acad Sci U S A 96:29–34. doi: 10.1073/pnas.96.1.29

Borau C, Kim T, Bidone T, et al. (2012) Dynamic mechanisms of cell rigidity sensing: insights from a computational model of actomyosin networks. PLoS One 7:e49174. doi: 10.1371/journal.pone.0049174

Borisy GG, Svitkina TM (2000) Actin machinery: pushing the envelope. Curr Opin Cell Biol 12:104–112. doi:10.1016/S0955-0674(99)00063-0

Broedersz CP, Mackintosh FC (2014) Modeling semiflexible polymer networks. Rev Mod Phys 86:995–1036. doi: 10.1103/RevModPhys.86.995

Bunnell SC, Kapoor V, Trible RP, et al. (2001) Dynamic actin polymerization drives T cell receptor-induced spreading: a role for the signal transduction adaptor LAT. Immunity 14:315–329. doi:10.1016/S1074-7613(01)00112-1

Carlier M, Pantaloni D, Korn E (1987) The mechanisms of ATP hydrolysis accompanying the polymerization of Mg- actin and Ca-actin. J Biol Chem 262:3052–3059.

Carlier MF, Pantaloni D, Korn ED (1986) The effects of Mg2+ at the high-affinity and low-affinity sites on the polymerization of actin and associated ATP hydrolysis. J Biol Chem 261:10785–10792.

Chennubhotla C, Rader AJ, Yang L-W, Bahar I (2005) Elastic network models for understanding biomolecular machinery: from enzymes to supramolecular assemblies. Phys Biol 2:S173–S180. doi: 10.1088/1478-3975/2/4/S12

731 Chu J-W, Voth GA (2006a) Coarse-grained modeling of the actin filament derived from
732 atomistic-scale simulations. Biophys J 90:1572–1582. doi: 10.1529/biophysj.105.073924

733 Chu J-W, Voth GA (2005) Allostery of actin filaments: molecular dynamics simulations and
734 coarse-grained analysis. Proc Natl Acad Sci U S A 102:13111–13116. doi:
735 10.1073/pnas.0503732102

736 Chu J-W, Voth GA (2006b) Coarse-grained modeling of the actin filament derived from
737 atomistic-scale simulations. Biophys J 90:1572–1582. doi: 10.1529/biophysj.105.073924

738 Clift R, Grace JR, Weber ME (2005) Bubbles, drops, and particles.

739 Cooper JA, Buhle EL, Walker SB, et al. (1983) Kinetic evidence for a monomer activation step
740 in actin polymerization. Biochemistry 22:2193–2202. doi: 10.1021/bi00278a021

741 De La Cruz EM, Roland J, McCullough BR, et al. (2010) Origin of twist-bend coupling in actin
742 filaments. Biophys J 99:1852–1860. doi: 10.1016/j.bpj.2010.07.009

743 Deriu MA, Bidone TC, Mastrangelo F, et al. (2011) Biomechanics of actin filaments: a
744 computational multi-level study. J Biomech 44:630–636. doi:
745 10.1016/j.jbiomech.2010.11.014

746 Deriu MA, Shkurti A, Paciello G, et al. (2012) Multiscale modeling of cellular actin filaments:
747 from atomistic molecular to coarse-grained dynamics. Proteins 80:1598–1609. doi:
748 10.1002/prot.24053

749 Doruker P, Atilgan AR, Bahar I (2000) Dynamics of proteins predicted by molecular dynamics
750 simulations and analytical approaches: application to alpha-amylase inhibitor. Proteins
751 40:512–524.

752 Durand P, Trinquier G, Sanejouand YH (1994) A new approach for determining low-frequency
753 normal modes in macromolecules. Biopolymers 34:759–771. doi: 10.1002/bip.360340608

754 Düttmann M, Mittnenzweig M, Togashi Y, et al. (2012) Complex intramolecular mechanics of
755 G-actin--an elastic network study. PLoS One 7:e45859. doi: 10.1371/journal.pone.0045859

756 Dykeman EC, Sankey OF (2010) Normal mode analysis and applications in biological physics. J
757 Phys Condens Matter 22:423202. doi: 10.1088/0953-8984/22/42/423202

758 Estes JE, Selden LA, Gershman LC (1987) Tight binding of divalent cations to monomeric actin.
759 Binding kinetics support a simplified model. J Biol Chem 262:4952–4957.
760 doi: 10.1016/S0006-3495(97)78232-8

761 Estes JE, Selden LA, Kinosian HJ, Gershman LC (1992a) Tightly-bound divalent cation of actin.
762 J Muscle Res Cell Motil 13:272–284. doi: 10.1007/BF01766455

763 Fan J, Saunders MG, Voth GA (2012) Coarse-graining provides insights on the essential nature
764 of heterogeneity in actin filaments. Biophys J 103:1334–1342. doi:
765 10.1016/j.bpj.2012.08.029

766 Flynn TC, Ma J (2004) Theoretical analysis of twist/bend ratio and mechanical moduli of
767 bacterial flagellar hook and filament. Biophys J 86:3204–3210. doi: 10.1016/S0006-
768 3495(04)74368-4

769 Fujii T, Iwane AH, Yanagida T, Namba K (2010) Direct visualization of secondary structures of
770 F-actin by electron cryomicroscopy. Nature 467:724–728. doi: 10.2142/biophys.51.260

771 Gardel ML, Nakamura F, Hartwig J, et al. (2006a) Stress-dependent elasticity of composite actin
772 networks as a model for cell behavior. Phys Rev Lett 96:088102. doi:
773 10.1103/PhysRevLett.96.088102

774 Gardel ML, Nakamura F, Hartwig JH, et al. (2006b) Prestressed F-actin networks cross-linked
775 by hinged filamins replicate mechanical properties of cells. Proc Natl Acad Sci U S A
776 103:1762–1767. doi: 10.1073/pnas.0504777103

777 Gittes F, Mickey B, Nettleton J, Howard J (1993) Flexural rigidity of microtubules and actin
778 filaments measured from thermal fluctuations in shape. J Cell Biol 120:923–934. doi:
779 10.1083/jcb.120.4.923

780 Golji J, Collins R, Mofrad MRK (2009) Molecular mechanics of the α-actinin rod domain:
781 Bending, torsional, and extensional behavior. PLoS Comput Biol. 5: e1000389. doi:
782 10.1371/journal.pcbi.1000389

783 Grooman B, Fujiwara I, Otey C, Upadhyaya A (2012) Morphology and viscoelasticity of actin
784 networks formed with the mutually interacting crosslinkers: palladin and alpha-actinin.
785 PLoS One 7:e42773. doi: 10.1371/journal.pone.0042773

786 Grudinin S, Redon S (2010) Practical modeling of molecular systems with symmetries. J
787 Comput Chem 31:1799–1814. doi: 10.1002/jcc.21434

788 Guan J-Q, Almo SC, Reisler E, Chance MR (2003) Structural reorganization of proteins revealed
789 by radiolysis and mass spectrometry: G-actin solution structure is divalent cation dependent.
790 Biochemistry 42:11992–12000. doi: 10.1021/bi034914k

791 Head DA, Levine AJ, MacKintosh FC (2003) Distinct regimes of elastic response and
792 deformation modes of cross-linked cytoskeletal and semiflexible polymer networks. Phys
793 Rev E Stat Nonlin Soft Matter Phys 68:061907. doi: 10.1103/PhysRevE.68.061907

794 Hess B, Bekker H, Berendsen HJC, Fraaije JGEM (1997) LINCS: A linear constraint solver for
795 molecular simulations. J Comput Chem 18:1463–1472. doi: 10.1002/(SICI)1096-
796 987X(199709)18:12<1463::AID-JCC4>3.0.CO;2-H

Hess B, Kutzner C, van der Spoel D, Lindahl E (2008) GROMACS 4: Algorithms for Highly Efficient, Load-Balanced, and Scalable Molecular Simulation. J Chem Theory Comput 4:435–447. doi: 10.1021/ct700301q

Hild G, Nyitrai M, Belágyi J, Somogyi B (1998) The influence of divalent cations on the dynamic properties of actin filaments: a spectroscopic study. Biophys J 75:3015–3022. doi: 10.1016/S0006-3495(98)77742-2

Hinsen K (2005) Normal mode theory and harmonic potential approximations. Norm. Mode Anal. Theory Appl. to Biol. Chem. Syst. pp 1–16. doi: 10.1201/9781420035070.ch1

Humphrey W, Dalke A, Schulten K (1996) VMD: Visual molecular dynamics. J Mol Graph 14:33–38. doi: 10.1016/0263-7855(96)00018-5

Isambert H, Venier P, Maggs AC, et al. (1995) Flexibility of actin filaments derived from thermal fluctuations. Effect of bound nucleotide, phalloidin, and muscle regulatory proteins. J Biol Chem 270:11437–11444. doi: 10.1074/jbc.270.19.11437

Janmey PA (1996) The Polyelectrolyte Nature of F-actin and the Mechanism of Actin Bundle Formation. J Biol Chem 271:8556–8563. doi: 10.1074/jbc.271.15.8556

Kabsch W, Mannherz HG, Suck D, et al. (1990) Atomic structure of the actin:DNase I complex. Nature 347:37–44. doi: 10.1038/347037a0

Kang H, Bradley MJ, McCullough BR, et al. (2012) Identification of cation-binding sites on actin that drive polymerization and modulate bending stiffness. Proc Natl Acad Sci U S A 109:16923–16927. doi: 10.1073/pnas.1211078109

Kim T (2014) Determinants of contractile forces generated in disorganized actomyosin bundles. Biomech Model Mechanobiol. doi: 10.1007/s10237-014-0608-2

Kim T, Hwang W, Kamm RD (2009a) Computational analysis of a cross-linked actin-like network. Exp Mech 49:91–104. doi: 10.1007/s11340-007-9091-3

Kim T, Hwang W, Kamm RD (2011) Dynamic role of cross-linking proteins in actin rheology. Biophys J 101:1597–1603. doi: 10.1016/j.bpj.2011.08.033

Kim T, Hwang W, Lee H, Kamm RD (2009b) Computational analysis of viscoelastic properties of crosslinked actin networks. PLoS Comput Biol 5:e1000439. doi: 10.1371/journal.pcbi.1000439

Kojima H, Ishijima A, Yanagida T (1994) Direct measurement of stiffness of single actin filaments with and without tropomyosin by in vitro nanomanipulation. Proc Natl Acad Sci U S A 91:12962–12966. doi: 10.1073/pnas.91.26.12962

Korn E, Carlier M, Pantaloni D (1987) Actin polymerization and ATP hydrolysis. Science (80-) 238:638–644. doi: 10.1126/science.3672117

Kwon HJ, Kakugo A, Shikinaka K, et al. (2005) Morphology of actin assemblies in response to polycation and salts. Biomacromolecules 6:3005–3009. doi: 10.1021/bm050320g

Lieleg O, Claessens MMAE, Bausch AR (2010) Structure and dynamics of cross-linked actin networks. Soft Matter 6:218-225. doi: 10.1039/b912163n

Lieleg O, Schmoller KM, Claessens MMAE, Bausch AR (2009) Cytoskeletal polymer networks: viscoelastic properties are determined by the microscopic interaction potential of cross-links. Biophys J 96:4725–4732. doi: 10.1016/j.bpj.2009.03.038

MacKintosh F, Käs J, Janmey P (1995) Elasticity of semiflexible biopolymer networks. Phys Rev Lett 75:4425–4428. doi: 10.1103/PhysRevLett.75.4425

Méjean C, Hué HK, Pons F, et al. (1988) Cation binding sites on actin: a structural relationship between antigenic epitopes and cation exchange. Biochem Biophys Res Commun 152:368–375. doi: 10.1016/S0006-291X(88)80723-X

Moraczewska J, Strzelecka-Gołaszewska H, Moens PD, dos Remedios CG (1996) Structural changes in subdomain 2 of G-actin observed by fluorescence spectroscopy. Biochem J 317 (Pt2):605–611.

Moraczewska J, Wawro B, Seguro K, Strzelecka-Golaszewska H (1999) Divalent cation-, nucleotide-, and polymerization-dependent changes in the conformation of subdomain 2 of actin. Biophys J 77:373–385. doi: 10.1016/S0006-3495(99)76896-7

Murakami K, Yasunaga T, Noguchi TQP, et al. (2010) Structural basis for actin assembly, activation of ATP hydrolysis, and delayed phosphate release. Cell 143:275–287. doi: 10.1016/j.cell.2010.09.034

Nyitrai M (1999) The flexibility of actin filaments as revealed by fluorescence resonance energy transfer. The Influence of divalent cations. J Biol Chem 274:12996–13001. doi: 10.1074/jbc.274.19.12996

Oda T, Iwasa M, Aihara T, et al. (2009) The nature of the globular- to fibrous-actin transition. Nature 457:441–445. doi: 10.1038/nature07685

Onck PR, Koeman T, Van Dillen T, Van Der Giessen E (2005) Alternative explanation of stiffening in cross-linked semiflexible networks. Phys Rev Lett. doi: 10.1103/PhysRevLett.95.178102

Oostenbrink C, Soares T a, van der Vegt NFA, Van Gunsteren WF (2005) Validation of the 53A6 GROMOS force field. Eur Biophys J 34:273–284. doi: 10.1007/s00249-004-0448-6

Orlova A, Egelman EH (1995) Structural dynamics of F-actin: I. Changes in the C terminus. J Mol Biol 245:582–597. doi: 10.1006/jmbi.1994.0048

Ott A, Magnasco M, Simon A, Libchaber A (1993) Measurement of the persistence length of polymerized actin using fluorescence microscopy. Phys Rev E. doi: 10.1103/PhysRevE.48.R1642

Otterbein LR, Graceffa P, Dominguez R (2001) The crystal structure of uncomplexed actin in the ADP state. Science 293:708–711. doi: 10.1126/science.1059700

Park J, Kahng B, Kamm RD, Hwang W (2006) Atomistic simulation approach to a continuum description of self-assembled beta-sheet filaments. Biophys J 90:2510–2524. doi: 10.1529/biophysj.105.074906

Pfaendtner J, Branduardi D, Parrinello M, et al. (2009) Nucleotide-dependent conformational states of actin. Proc Natl Acad Sci U S A 106:12723–12728. doi: 10.1073/pnas.0902092106

Pfaendtner J, De La Cruz EM, Voth GA (2010) Actin filament remodeling by actin depolymerization factor/cofilin. Proc Natl Acad Sci U S A 107:7299–7304. doi: 10.1073/pnas.0911675107

Saunders MG, Voth GA (2012) Comparison between actin filament models: coarse-graining reveals essential differences. Structure 20:641–653. doi: 10.1016/j.str.2012.02.008

Scharf RE, Newman J (1995) Mg- and Ca-actin filaments appear virtually identical in steady-state as determined by dynamic light scattering. Biochim Biophys Acta 1253:129–132. doi: 10.1016/0167-48380167-4838(95)00186-5

Schmoller KM, Lieleg O, Bausch AR (2009) Structural and viscoelastic properties of actin/filamin networks: Cross-linked versus bundled networks. Biophys J 97:83–89. doi: 10.1016/j.bpj.2009.04.040

Schnurr B, Gittes F, MacKintosh FC, Schmidt CF (1997) Determining Microscopic Viscoelasticity in flexible and semiflexible polymer networks from thermal fluctuations. Macromolecules 30:7781–7792. doi: 10.1021/ma970555n

Selden LA, Estes JE, Gershman LC (1983) The tightly bound divalent cation regulates actin polymerization. Biochem Biophys Res Commun 116:478–485. doi: 10.1016/0006-291X(83)90548-X

Shi W, Inamdar MV, Sastry AM, Lastoskie CM (2007) Divalent cation adsorption on the actin monomer. J Phys Chem C 111:15642–15652. doi: 10.1021/jp073763i

Shin JH, Gardel ML, Mahadevan L, et al. (2004) Relating microstructure to rheology of a bundled and cross-linked F-actin network in vitro. Proc Natl Acad Sci U S A 101:9636–9641. doi: 10.1073/pnas.0308733101

Splettstoesser T, Noé F, Oda T, Smith JC (2009) Nucleotide-dependence of G-actin conformation from multiple molecular dynamics simulations and observation of a putatively polymerization-competent superclosed state. Proteins 76:353–364. doi: 10.1002/prot.22350

Steinmetz MO, Goldie KN, Aebi U (1997) A correlative analysis of actin filament assembly, structure, and dynamics. J Cell Biol 138:559–574. doi: 10.1083/jcb.138.3.559

Strzelecka-Gołaszewska H, Moraczewska J, Khaitlina SY, Mossakowska M (1993) Localization of the tightly bound divalent-cation-dependent and nucleotide-dependent conformation changes in G-actin using limited proteolytic digestion. Eur J Biochem 211:731–742. DOI: 10.1111/j.1432-1033.1993.tb17603.x

Strzelecka-Golaszewska H, Wozniak A, Hult T, Lindberg U (1996) Effects of the type of divalent cation, Ca2+ or Mg2+, bound at the high-affinity site and of the ionic composition of the solution on the structure of F-actin. Biochem J 316 (Pt3):713–721.

Tama F, Gadea FX, Marques O, Sanejouand YH (2000) Building-block approach for determining low-frequency normal modes of macromolecules. Proteins Struct Funct Genet 41:1–7. doi: 10.1002/1097-0134(20001001)41:1<1::AID-PROT10>3.0.CO;2-P

Tharmann R, Claessens M, Bausch A (2007) Viscoelasticity of isotropically cross-linked actin networks. Phys Rev Lett 98:088103. doi: 10.1103/PhysRevLett.98.088103

Tirion MM (1996) Large amplitude elastic motions in proteins from a single-parameter, atomic analysis. Phys Rev Lett 77:1905–1908. doi: 10.1103/PhysRevLett.77.1905

Tseng Y, Schafer BW, Almo SC, Wirtz D (2002) Functional synergy of actin filament cross-linking proteins. J Biol Chem 277:25609–25616. doi: 10.1074/jbc.M202609200

Unterberger MJ, Schmoller KM, Bausch AR, Holzapfel GA (2013) A new approach to model cross-linked actin networks: Multi-scale continuum formulation and computational analysis. J Mech Behav Biomed Mater 22:95–114. doi: 10.1016/j.jmbbm.2012.11.019

Wagner B, Tharmann R, Haase I, et al. (2006) Cytoskeletal polymer networks: the molecular structure of cross-linkers determines macroscopic properties. Proc Natl Acad Sci U S A 103:13974–13978. doi: 10.1073/pnas.0510190103

Wang N, Butler J, Ingber D (1993) Mechanotransduction across the cell surface and through the cytoskeleton. Science 260:1124–1127. doi: 10.1126/science.7684161

Wriggers W, Schulten K (1997) Stability and dynamics of G-actin: back-door water diffusion and behavior of a subdomain 3/4 loop. Biophys J 73:624–639. doi: 10.1016/S0006-3495(97)78098-6

928 Xu J, Tseng Y, Wirtz D (2000) Strain hardening of actin filament networks: regulation by the
929 dynamic cross-linking protein {alpha}-actinin. J Biol Chem 275:35886–35892. doi:
930 10.1074/jbc.M002377200

931 Yang L-W, Chng C-P (2008) Coarse-grained models reveal functional dynamics--I. Elastic
932 network models--theories, comparisons and perspectives. Bioinform Biol Insights 2:25–45.

933 Zimmerle CT, Patane K, Frieden C (1987) Divalent cation binding to the high- and low-affinity
934 sites on G-actin. Biochemistry 26:6545–6552. DOI: 10.1021/bi00394a039

935

FIGURE LEGENDS

Fig. 1 Atomic and coarse grain models of monomer subunits, F-actin and actin network. (a) Ribbon structure of the energy-minimized monomer subunit in the ADP-bound configuration (with folded DB loop). The positions of the six crystallographic calcium binding sites, labeled CA382-CA387, are shown as the red spheres. The position of the ADP nucleotide, near the high-affinity calcium binding site CA382, is denoted in licorice representation. (b) Ribbon representation of the 13-monomer repeat unit of F-actin used as input for MD simulation. Each monomer subunit is shown in a different color. For clarity, the intra-crystalline water is not shown. (c) Ribbon representation of the 13-monomer F-actin within the solvated rectangular box used for equilibrium MD. The filament is represented as "infinite" to account for PBC. (d) Filament corresponding to the one in (c), represented as "infinite". (e) Schematics of the ENM model of F-actin, where each Cα atom is replaced by a node. (f) RTB model of F-actin, with rigid blocks corresponding to the four functional subdomains (SD1-4) of actin, in order to preserve the basic subunit topology at the filament level. (g) Coarse-graining scheme and mechanics of the actin filaments and ACPs: actin filaments comprise a series of cylindrical segments with barbed and pointed ends; ACPs have two arms in parallel, rigidly bound to the actin filament. Equilibrium lengths and angles are governed by various extensional (k_s) and bending (k_f) rigidities. (h) A schematic view of the simulated shear strain test. A rigidly crosslinked actin filament network is pinned at the –z boundary and a constant shear strain is applied to the free +z boundary

Fig. 2 Inter- and intra-strand distances between mass centers of subdomains.
(a) An actin trimer is shown in coarse-grained (CG) and atomistic (Ribbon) representations. The four subdomains labeled are: SD1 (Blue) residues 1-32, 70-144, 338-375; SD2 (Red) residues 33-69; SD3 (Green) residues 145-180 and 270-337; and SD4 (Purple) residues 181-269. (b) F-actin radius decreased in all systems during MD simulations, and in particular with saturation of cation binding, for both ADP- and ATP-F-actins. Cross-strand interactions are reported in terms of distances between the mass centers of SD1/SD1 (c), and SD4/SD1 (d). The distances between SD4/SD1 and SD1/SD1 decrease within 12 ns of equilibrium MD simulations, leading to a compaction of the subunit residues towards the F-actin longitudinal axis. In ADP-F-actin, saturation of cation binding always lead to lesser variability in the distances between SD4/SD1 and SD1/SD1 (reduced standard deviation from their average values). (e) Average and standard deviation of the intra-strand distances between SD2 and SD1 pertaining to monomers *(i)* and *(i+2)*, respectively, show that occupancy of both high- and low-affinity binding sites of the subunits renders F-actin more homogeneous in the pairing of longitudinal subunits

Fig. 3. Molecular rearrangements of monomer subunits related with variations in their relative positioning. (a) Ribbon representation of the monomer subunit with spheres representing the four functional subdomains, and the dihedral angle between the planes with vertices in SD1-SD2-SD3 and SD1-SD3-SD4, highlighted with a red arrow. (b) Average and standard deviation of the dihedral angle, computed as the angle between the plane defined by the mass centers of SD1, SD2 and SD3 and the plane defined by the mass centers of SD1, SD3 and SD4, show that saturation of cation binding lead to greater variability in the structure of F-actin. (c) Root Mean Square (RMS) fluctuations of selected residue groups: the DB loop, including residues 38-52, is the most highly fluctuating group in the subunits; the nucleotide has high fluctuation in ADP-Pi. (d) Intra-monomer distances between SD2 and SD4 provide a mean to

evaluate relative repositioning of the two subunits upon nucleotide hydrolysis: this distance is enhanced for ADP-F-actin and influences the cleft size. (e) The 3D distance between the centers of mass of the protein backbone of residues 57-69, 30-33 in SD2 and 203-216 in SD4, residues internal to the nucleotide cleft

Fig. 4 Persistence lengths and extensional rigidities of F-actins. (a**)** Persistence length shows changes up to 10% in ATP-F-actins and up to 6% in ADP-F-actins, depending upon the presence and the type of one or multiple cations at the high-, intermediate- and low-affinity binding sites (n = 10 simulations, error bar: standard error). (b) Changes observed in extensional rigidity of F-actin mirrored those of persistence length, except that in the case of Ca^{2+} saturation ATP-F-actin was more rigid in bending than ADP-F-actin but less rigid in stretching than ADP-F-actin (n=10 simulations, error bar: standard error). (c) Normalized standard deviation of the root mean square distance (σ_{RMSD}) of the Cα of the monomer subunits from the average monomer structure.

Fig. 5 Strain-induced stiffening curves from the crosslinked actin network. (a-b) Strain-stiffening response of the crosslinked actin network with 11 different nucleotide/cation bound forms, including the intermediate ADP-Pi, with compliant and rigid ACPs, $k_{s,ACP}$=0.002 N/m and 0.2 N/m. (c-d) Strain-induced stiffening of the crosslinked actin filament network resulting from altered mechanics of F-actin when Mg^{2+} is bound at the "stiffness" site (Kang et al. 2012), with $ks,_{ACP}$=0.002 N/m and 0.2 N/m. (e-f) Stress at high deformation, 60% strain, as a function of F-actin persistence lengths resulting from binding of Mg^{2+} at the stiffness site, at $ks,_{ACP}$=0.002 N/m and 0.2 N/m (Kang et al. 2012)

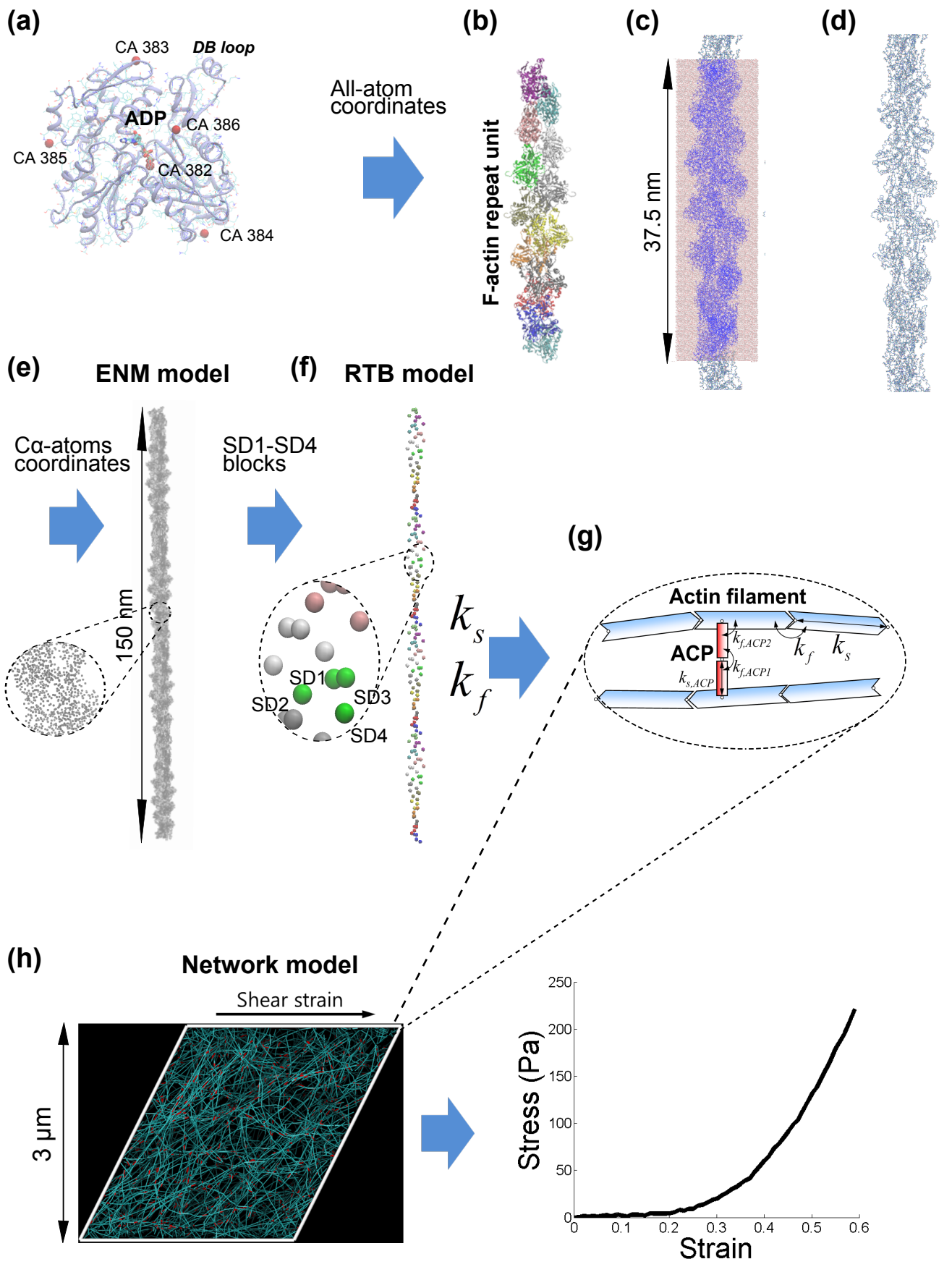
(a)
CA 383
DB loop
ADP
CA 386
CA 385
CA 382
CA 384
All-atom coordinates
(b)
F-actin repeat unit
(c)
37.5 nm
(d)
(e)
ENM model
Cα-atoms coordinates
150 nm
(f)
RTB model
SD1-SD4 blocks
SD1
SD2
SD3
SD4
k_s
k_f
(g)
Actin filament
ACP
$k_{f,ACP2}$
$k_{f,ACP1}$
$k_{s,ACP}$
k_f
k_s
(h)
Network model
Shear strain
3 μm
Stress (Pa)
Strain
0
50
100
150
200
250
0
0.1
0.2
0.3
0.4
0.5
0.6

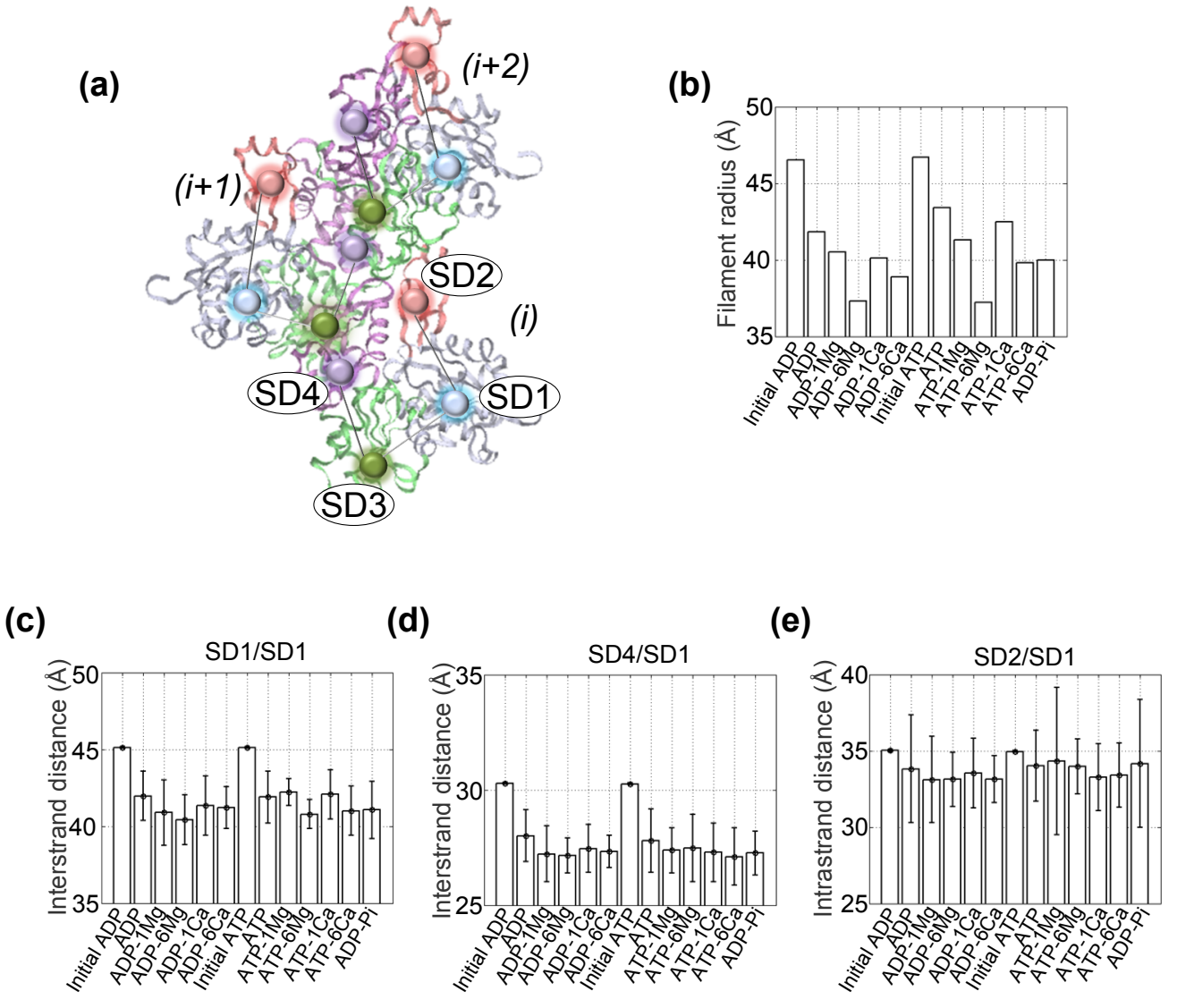
(a)
(i+2)
(i+1)
SD2
(i)
SD4
SD1
SD3
(b)
Filament radius (Å)
50
45
40
35
Initial ADP
ADP
ADP-1Mg
ADP-6Mg
ADP-1Ca
ADP-6Ca
Initial ATP
ATP
ATP-1Mg
ATP-6Mg
ATP-1Ca
ATP-6Ca
ADP-Pi
(c)
SD1/SD1
Interstrand distance (Å)
50
45
40
35
(d)
SD4/SD1
Interstrand distance (Å)
35
30
25
(e)
SD2/SD1
Intrastrand distance (Å)
40
35
30
25

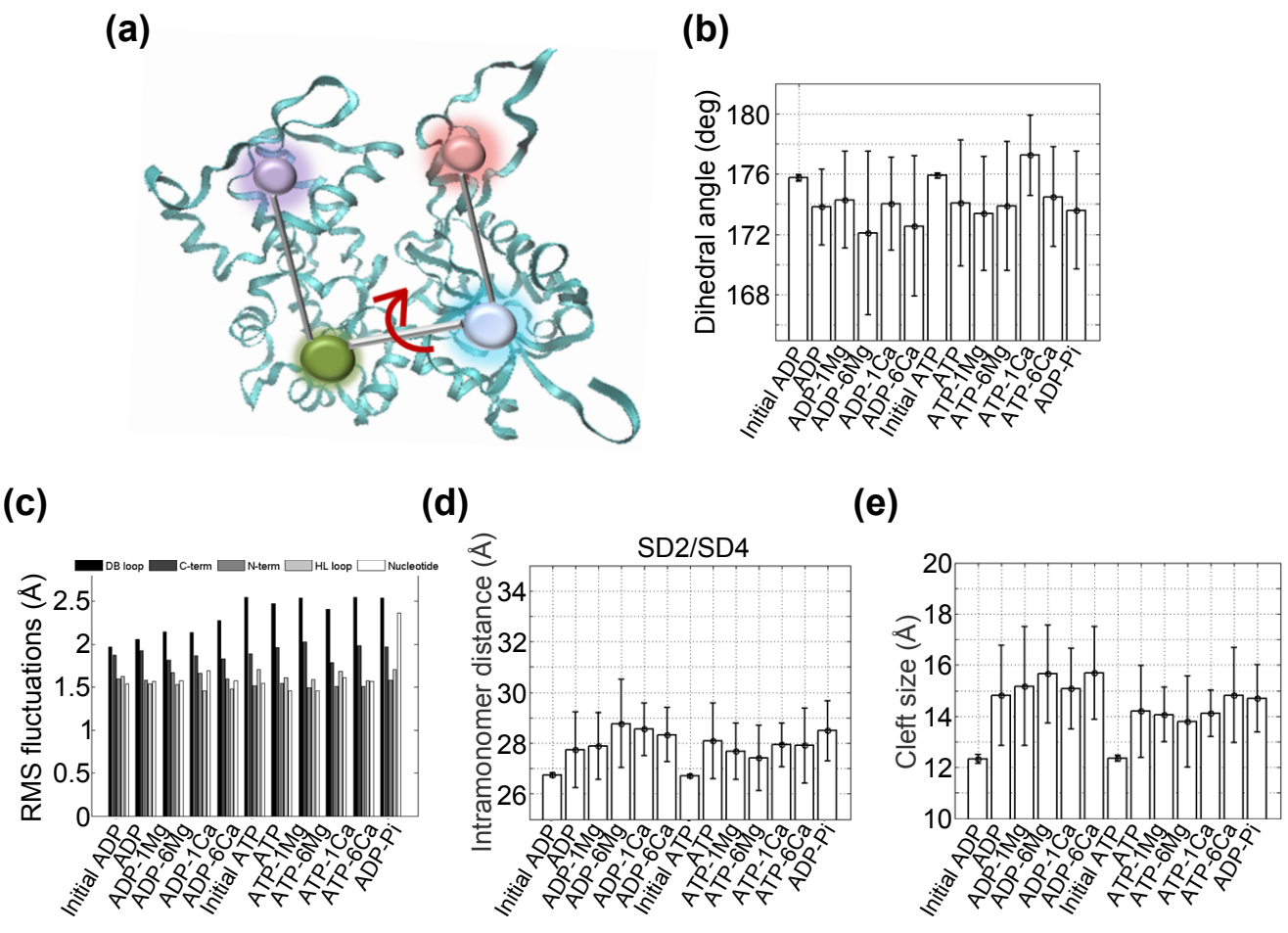
(a)
(b)
Dihedral angle (deg)
180
176
172
168
Initial ADP
ADP
ADP-1Mg
ADP-6Mg
ADP-1Ca
ADP-6Ca
Initial ATP
ATP
ATP-1Mg
ATP-6Mg
ATP-1Ca
ATP-6Ca
ADP-Pi
(c)
DB loop
C-term
N-term
HL loop
Nucleotide
RMS fluctuations (Å)
2.5
2
1.5
1
0.5
0
(d)
SD2/SD4
Intramonomer distance (Å)
34
32
30
28
26
(e)
Cleft size (Å)
20
18
16
14
12
10

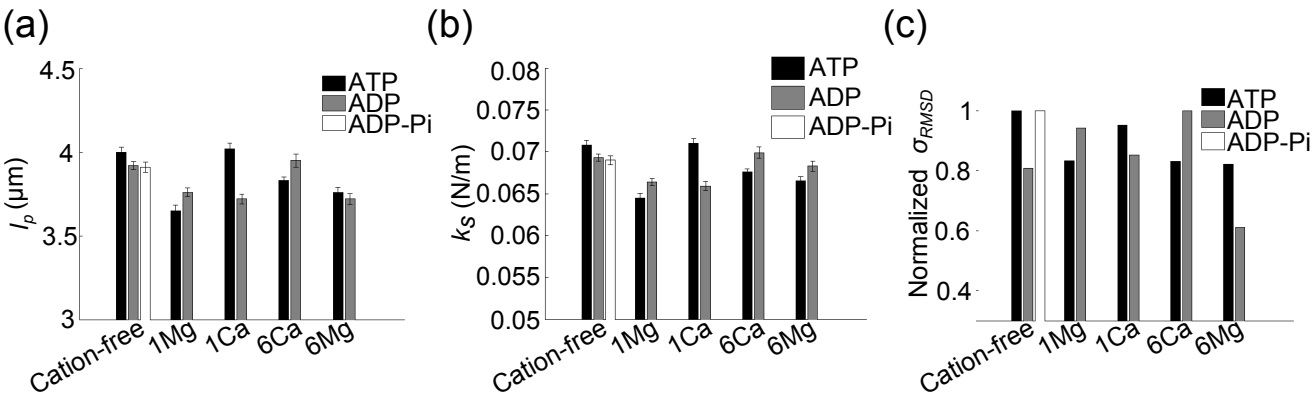
(a)
(b)
(c)
ATP
ADP
ADP-Pi
l_p (μm)
k_S (N/m)
Normalized σ_{RMSD}
4.5
4
3.5
3
0.08
0.075
0.07
0.065
0.06
0.055
0.05
1
0.8
0.6
0.4
Cation-free
1Mg
1Ca
6Ca
6Mg

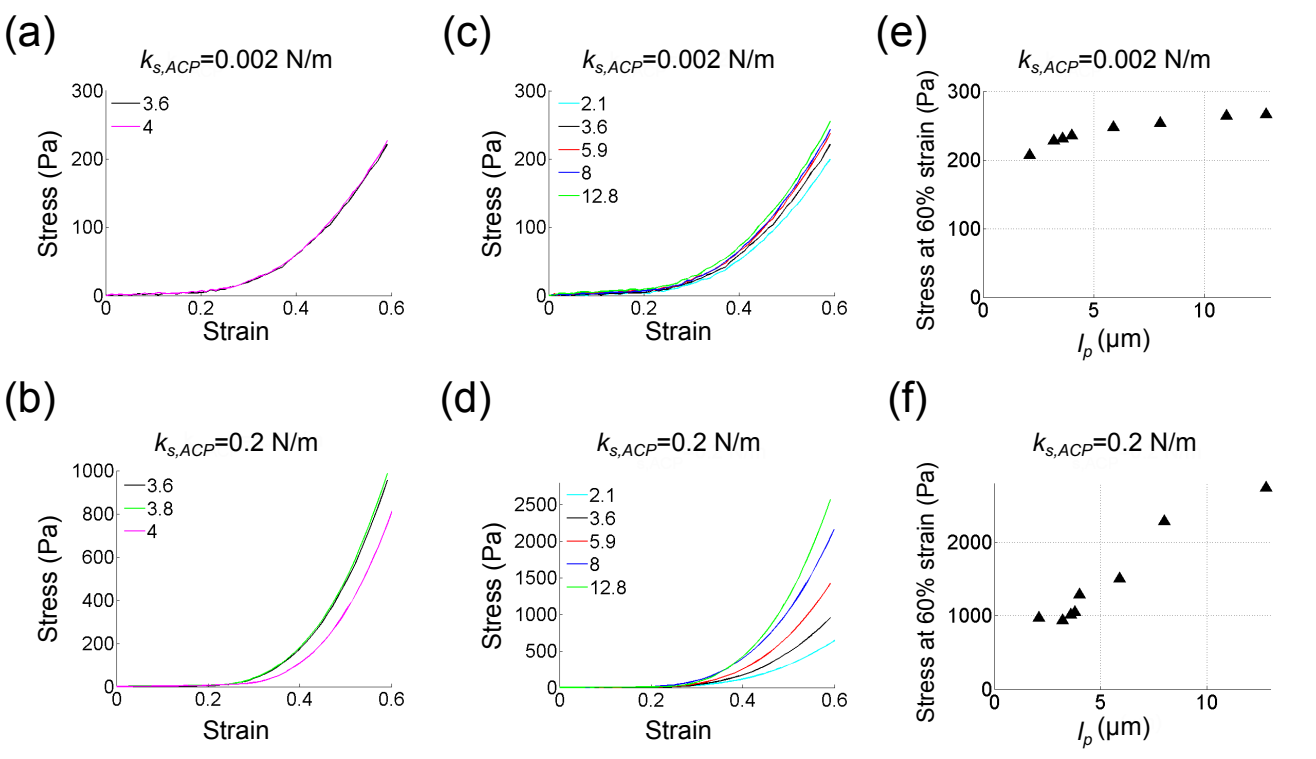
(a)
$k_{s,ACP}$=0.002 N/m
3.6
4
Stress (Pa)
Strain
(b)
$k_{s,ACP}$=0.2 N/m
3.6
3.8
4
Stress (Pa)
Strain
(c)
$k_{s,ACP}$=0.002 N/m
2.1
3.6
5.9
8
12.8
Stress (Pa)
Strain
(d)
$k_{s,ACP}$=0.2 N/m
2.1
3.6
5.9
8
12.8
Stress (Pa)
Strain
(e)
$k_{s,ACP}$=0.002 N/m
Stress at 60% strain (Pa)
l_p (μm)
(f)
$k_{s,ACP}$=0.2 N/m
Stress at 60% strain (Pa)
l_p (μm)

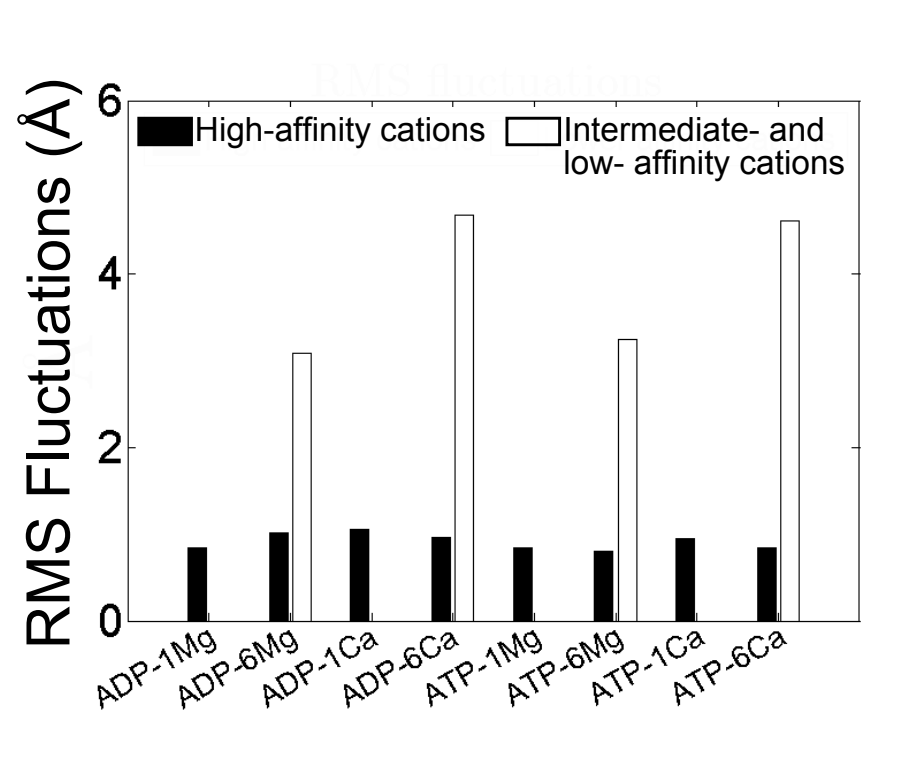
RMS Fluctuations (Å)
6
4
2
0
High-affinity cations
Intermediate- and low- affinity cations
ADP-1Mg
ADP-6Mg
ADP-1Ca
ADP-6Ca
ATP-1Mg
ATP-6Mg
ATP-1Ca
ATP-6Ca

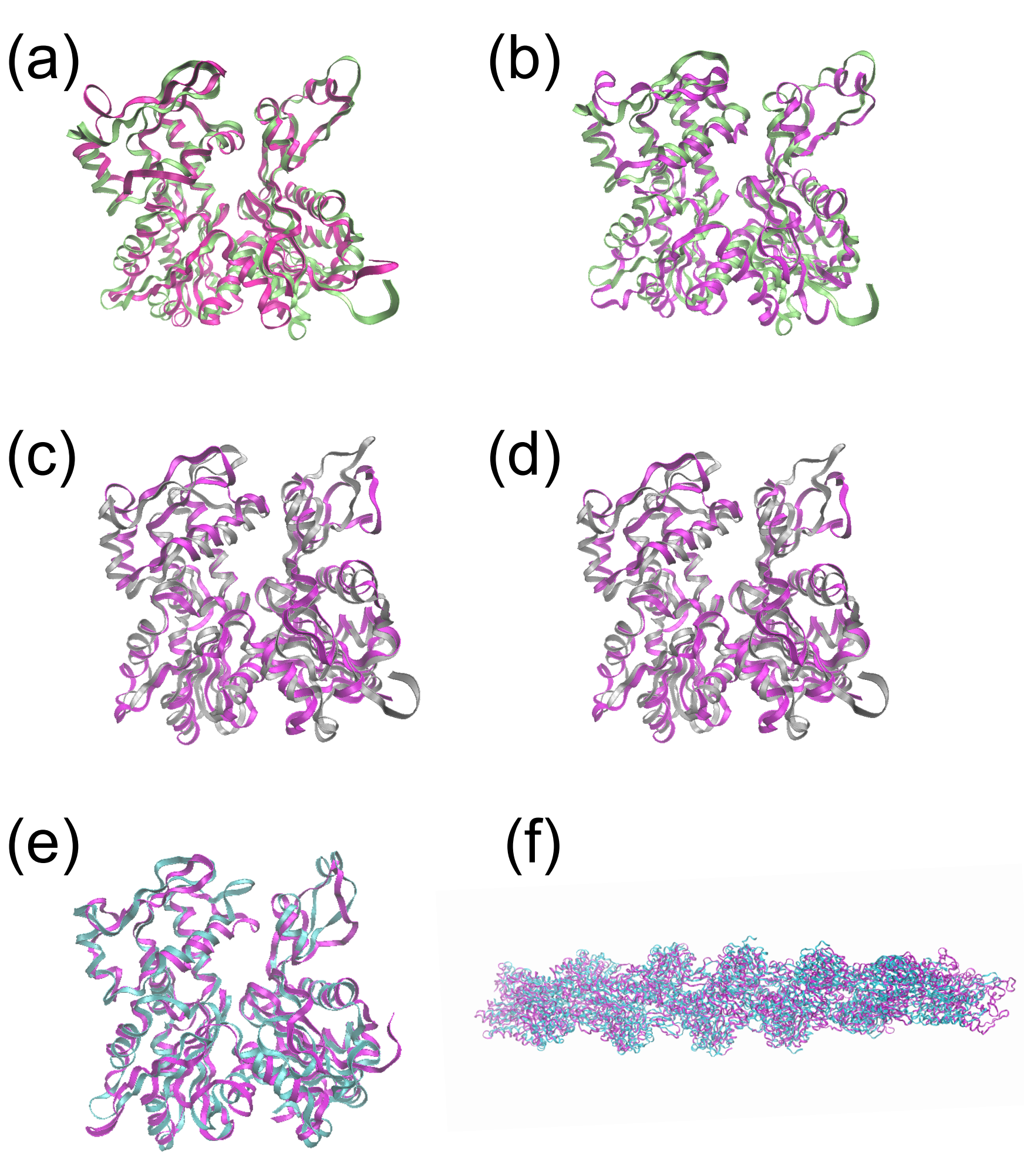
(a)
(b)
(c)
(d)
(e)
(f)